Article

Cell Reports

Nanobody-mediated macromolecular crowding induces membrane fission and remodeling in the African trypanosome

Graphical abstract

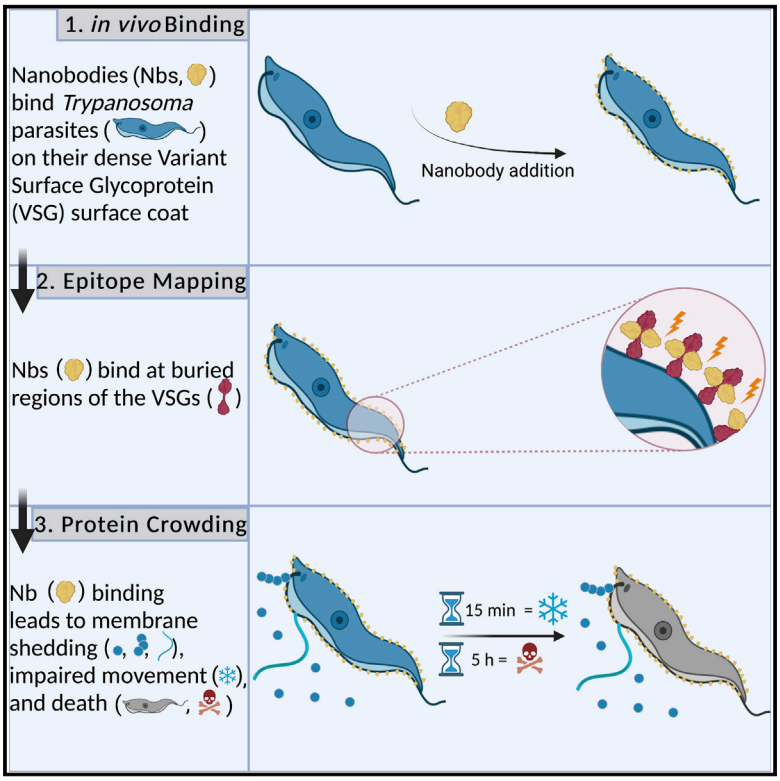

Highlights

- Anti-VSG nanobodies (Nbs) can bind deep into the VSG coat of living trypanosomes
- Higher-affinity Nbs are linked to larger surface areas of interaction
- High-affinity binding of VSG Nbs can affect VSG diffusion and cell motility
- Nb binding can lead to molecular crowding-mediated shedding of the cell surface

Authors

Alexander Hempelmann, Laura Hartleb, Monique van Straaten, ..., Markus Engstler, C. Erec Stebbins, Nicola G. Jones

Correspondence

e.stebbins@dkfz-heidelberg.de (C.E.S.), nicola.jones@uni-wuerzburg.de (N.G.J.)

In brief

Hempelmann et al. analyze effects of anti-VSG nanobodies (Nbs) on African trypanosomes. Employing techniques spanning structural biology and cellular dynamics, they identify one Nb that binds with high affinity and causes molecular crowding, resulting in a perturbation of protein diffusion and cell motility with shedding of the surface coat.

Hempelmann et al., 2021, Cell Reports *37*, 109923
November 2, 2021
https://doi.org/10.1016/j.celrep.2021.109923

CellPress

Cell Reports

CellPress
OPEN ACCESS

Article

Nanobody-mediated macromolecular crowding induces membrane fission and remodeling in the African trypanosome

Alexander Hempelmann,[1] Laura Hartleb,[2] Monique van Straaten,[1] Hamidreza Hashemi,[3] Johan P. Zeelen,[1] Kevin Bongers,[2] F. Nina Papavasiliou,[3] Markus Engstler,[2] C. Erec Stebbins,[1,4,*] and Nicola G. Jones[2,*]

[1]Division of Structural Biology of Infection and Immunity, German Cancer Research Center, Heidelberg 69120, Germany

[2]Department of Cell and Developmental Biology, Theodor-Boveri-Institute, Biocenter, Julius-Maximilians-Universität of Würzburg, Würzburg 97074, Germany

[3]Division of Immune Diversity, German Cancer Research Center, Heidelberg 69120, Germany

[4]Lead contact

*Correspondence: e.stebbins@dkfz-heidelberg.de (C.E.S.), nicola.jones@uni-wuerzburg.de (N.G.J.)

https://doi.org/10.1016/j.celrep.2021.109923

SUMMARY

The dense variant surface glycoprotein (VSG) coat of African trypanosomes represents the primary host-pathogen interface. Antigenic variation prevents clearing of the pathogen by employing a large repertoire of antigenically distinct VSG genes, thus neutralizing the host's antibody response. To explore the epitope space of VSGs, we generate anti-VSG nanobodies and combine high-resolution structural analysis of VSG-nanobody complexes with binding assays on living cells, revealing that these camelid antibodies bind deeply inside the coat. One nanobody causes rapid loss of cellular motility, possibly due to blockage of VSG mobility on the coat, whose rapid endocytosis and exocytosis are mechanistically linked to *Trypanosoma brucei* propulsion and whose density is required for survival. Electron microscopy studies demonstrate that this loss of motility is accompanied by rapid formation and shedding of nanovesicles and nanotubes, suggesting that increased protein crowding on the dense membrane can be a driving force for membrane fission in living cells.

INTRODUCTION

Trypanosoma brucei causes African sleeping sickness in humans and nagana in cattle. These pathogens possess a densely packed surface coat populated almost entirely by the variant surface glycoprotein (VSG) in the mammalian-infectious forms of the parasite. As *T. brucei* is an extracellular pathogen, the VSG coat is extensively exposed to the immune system and is the primary surface of interaction within the host. It is also highly antigenic, inducing robust antibody-mediated responses that are neutralizing (Borst, 2002; Overath et al., 1994). However, parasites possess a genetic repertoire of antigenically distinct VSGs (2,000+ genes and pseudogenes), allowing individual parasites to switch the coat to another variant, thus creating a novel surface array to which the immune system is naive and must re-adapt. This process of antigenic variation repeats with recurring cycles of parasite clearance, coat switching, and pathogen re-growth (Bangs, 2018).

Trypanosomes employ a second immune evasion mechanism, antibody clearance and subsequent recycling of VSG molecules. This process helps evasion of complement-mediated immune destruction but is only effective at low antibody titers (Engstler et al., 2007; Horn, 2014; Mugnier et al., 2016; Pal et al., 2003). Facilitated by the remarkably high endocytosis rate at the flagellar pocket (FP), anti-VSG antibodies are selectively removed from VSG molecules within minutes (Engstler et al., 2004; Webster et al., 1990). This requires high mobility of the VSG molecules and free lateral diffusion (Bülow et al., 1988; Hartel et al., 2016, 2015).

VSGs are glycosylated proteins of roughly 60 kDa and are comprised of two subdomains: a long, rod-like N-terminal domain (NTD) spanning approximately 350 aa followed by a C-terminal domain (CTD) of roughly 100 aa that attaches to the glycophosphatidylinositol (GPI) anchor, which links the protein to the membrane. The NTDs are composed of a tightly packed three-helix bundle decorated with extended insertions that produce top and bottom "lobes" at polar ends of the rod-like, helical scaffolding. Despite decades of research, very little is known about the interactions of immune proteins with the VSG coat. Few studies have mapped any defined natural epitopes and at present no antibody-VSG co-crystal structures exist. Reviewing multiple indirect studies (involving monoclonal antibodies, nanobodies [Nbs], polyclonal antisera, lectins, and proteases), Schwede et al. (2015) proposed that contrary to many discussions in published literature, a substantial portion of the NTD (ending at the bottom lobe) of the VSGs could be accessible to the immune system.

In order to address this topic, we pursued structural studies of several camelid Nbs raised to the VSG coat (derived from

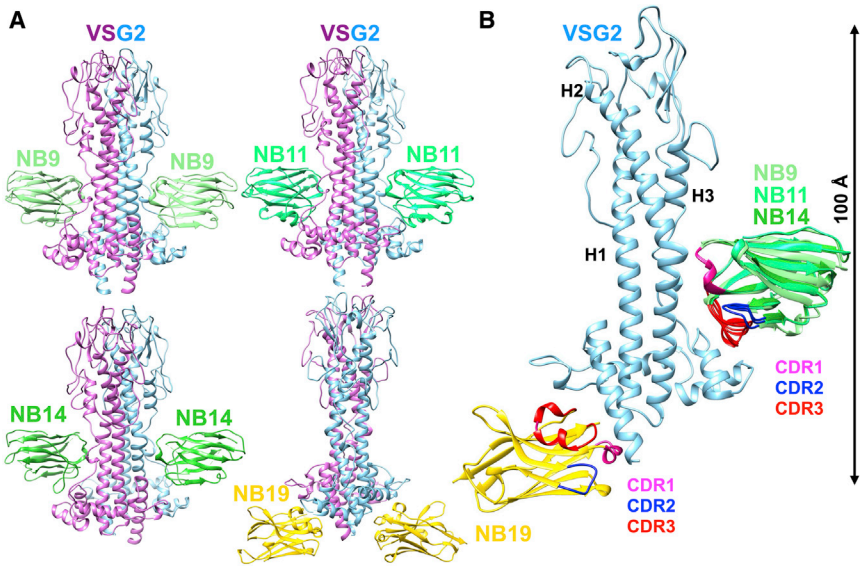

Figure 1. Overall structures of VSG2-Nb complexes

(A) The four nanobody (Nb)-VSG2 structures with $NB9_{VSG2}$ (NB9 in light green, top left), $NB11_{VSG2}$ (NB11 in lime green, top right), $NB14_{VSG2}$ (NB14 in green, bottom left), and $NB19_{VSG2}$ (NB19 in gold, bottom right), as well as VSG2 (dimer in cyan/purple), are depicted as ribbon diagrams.

(B) Superposition of VSG2-Nb complexes. The complementarity-determining regions (CDRs) are shown in magenta (CDR1), blue (CDR2), and red (CDR3). Structures are illustrated with Chimera (Pettersen et al., 2004).

camelid antibodies produced through VSG vaccination). These provide both a biologically relevant context (as *T. brucei*-related species cause surra in camelids [Radwanska et al., 2018]), as well as a system generally amenable to crystallographic analysis (de Marco, 2011). Previous studies have shown that high-affinity Nbs can be effectively raised to VSGs (Arbabi-Ghahroudi, 2017). Addition of such Nbs to AnTat1.1-expressing *T. brucei* was shown to induce trypanosome lysis even in the absence of the effector Fc domain (Stijlemans et al., 2017). Addition of the Nb initiated quick immobilization of trypanosomes, enlargement of the FP, and a major blockage of endocytosis. However, the mechanism mediating these phenomena has remained obscure. Our work sheds light on Nb action in the dense VSG coat and complements and explains previous observations in unexpected ways.

RESULTS

VSG2-Nb complexes

Nbs were generated from llamas immunized with the NTD of VSG2 (also known as VSG221 or VSG MITat1.2). To ensure that the antibody clones isolated from B cells were able to bind within surface coats and not only to the soluble form of the VSG, a filtering step of panning the library of VHH clones expressed by phage against intact UV-inactivated trypanosomes was added, and all clones were scored by flow cytometry analysis of such trypanosomes (STAR Methods; Figure S1A). From this we obtained a library of 69 distinct Nbs (belonging to 30 different complementarity-determining region [CDR]3 groups or B cell lineages). We initially crystallized three different clones ($NB9_{VSG2}$, $NB11_{VSG2}$, and $NB14_{VSG2}$) complexed to VSG2 (Figure 1; STAR Methods; Figure S1B; Tables S1 and S2). Those structures revealed that all of the Nbs bound similarly to the same epitope region and possessed a highly conserved consensus set of amino acids in the CDR1 and CDR3 loops that characterized most clones in the library, despite being derived from independent B cell lineages (discussed below). To identify other binding modalities, we searched for clones in our library with the most divergent CDRs. A few such were identified, and we crystallized one of these ($NB19_{VSG2}$), which indeed bound in a distinct location on VSG2. However, unexpectedly, this was not on the top, putative antigenic surface of the molecule, but nearly 100 Å down from the upper surface at the bottom of the NTD and adjacent to the postulated location of the CTD (Bartossek et al., 2017). The overall structure of VSG2 is not significantly changed from that previously reported (Freymann et al., 1990), aligning with a root-mean-square deviation in 1,440 atomic positions of 0.5 Å (single monomer).

Nbs bind deep into the VSG coat

Three of the Nbs ($NB9_{VSG2}$, $NB11_{VSG2}$, and $NB14_{VSG2}$) bind in an identical position. The binding site is approximately 60 Å down from the upper lobe of VSG2 and formed by a concave surface on the VSG three-helix bundle about midway down the length of the rod-like NTD (Figures 1A and 1B). This is consistent with a hypothesis that Nbs are more likely to bind concave or convex surfaces than flat ones (Stijlemans et al., 2004). Numerous side chains from the second two helices of the helical bundle make contacts to the Nbs (residues spanning 100–115 and 280–302 of VSG2), with the primary contacts solvent-facing, predominantly hydrophilic residues (e.g., Q111, T112, A285, E286, T301, and D313) as well as several minor side chain contacts and backbone contacts (Figure 2A). These Nbs interact with VSG2 through their variable CDR1 and CDR3 loops (without any significant contacts from the CDR2 loop) with a consensus set of side chains (CDR1 residues T28, S30, and N31 and CDR3 residues L100, L101, and S103) (Figures 2A and 2C). In contrast, $NB19_{VSG2}$ binds underneath the bottom lobe of VSG2 purely through CDR3 (Figure 2B). The contacts are a mixture of hydrophobic and polar interactions, but with a preponderance of aromatic side chain stacking (π-stacking) interactions involving residues W102, W112, and Y115 of $NB19_{VSG2}$ with the side chains Y375 and Y376 of VSG2.

Nb binding is detectable on living parasites

In order to examine the physiological relevance of these Nbs and their unexpected binding sites on VSG2, we performed a series

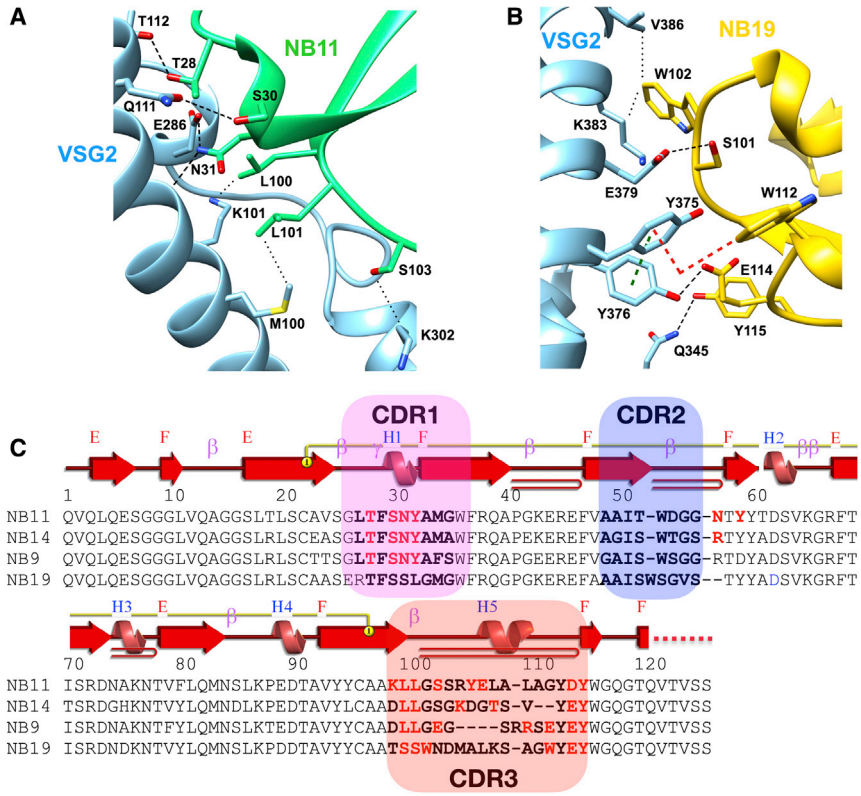

Figure 2. Interactions of Nb CDR variable loops with VSG2

(A) Interaction of the CDR3 loop from $NB11_{VSG2}$ with VSG2. Side chains from each protein have carbon atoms colored to match the main chain's ribbon, with atoms of oxygen, nitrogen, and sulfur shown in red, blue, and yellow, respectively. Hydrogen bonds and non-covalent bonds are shown as black squares and black dots, respectively.

(B) Interaction of the CDR3 loop from NB19 with VSG2.

(C) Sequence alignment and annotation of the four Nbs (numbering is for $NB11_{VSG2}$), including secondary structural elements, are shown together with highlighted regions of the CDR variable loops (colored as in Figure 1B). Residues that make contacts with VSG2 are shown with red letters. Structures are illustrated with Chimera (Pettersen et al., 2004) and secondary structure with PDBSum (de Beer et al., 2014).

of binding experiments to living trypanosomes (Figure 3; Figure S2). Nbs harboring a C-terminal hexa-histidine (6×His) tag were added to trypanosomes expressing different VSGs and the cells were analyzed with an anti-tag monoclonal antibody by fluorescence-activated cell sorting (FACS) (STAR Methods; Figure 3). Nbs $NB9_{VSG2}$, $NB11_{VSG2}$, and $NB14_{VSG2}$ were easily detected as binding to VSG2-expressing cells with several logs difference in signal (Figure 3A), whereas no binding could be detected for $NB19_{VSG2}$. In contrast, Nbs did not bind other VSGs (Figures 3B–3D), thereby showing high specificity ($NB11_{VSG2}$ shown as an example). To verify that the surface accessibility is not only limited to the relatively small Nbs, we created a sortaggable variant of the camelid heavy chain immunoglobulin (Ig)G2 antibody with the corresponding $NB11_{VSG2}$ Ig domain and found it can, in fact, bind the live parasite coat (Figure S2A).

The inability to detect $NB19_{VSG2}$ raised the possibility that the binding we observed in solution and in the crystal structure was an artifact of using the soluble VSG2 as the antigen for immunization. A second possibility was that the deep binding we observe in the crystal structure buries $NB19_{VSG2}$ beyond the reach of the anti-His IgG antibodies. To distinguish between these two models, we directly labeled $NB19_{VSG2}$ and other Nbs with fluorescent moieties. In one case we chemically conjugated the fluorophore fluorescein isothiocyanate (FITC) to the proteins (to free amine groups, typically exposed lysine residues), showing that the Nbs generally could be detected and also how they compare to a full anti-VSG2 IgG (Figure 3E). While only a small shift in fluorescence intensity can be observed for $NB19_{VSG2}$-FITC (compared to the non-stained sample, Figure 3E), it showed significance in a two-tailed t test ($p = 0.0109$, Figure S2M). To further probe binding, we sought to avoid whole-scale chemical labeling of proteins (and possible artifacts of that), and turned to a single, site-specific covalent modification of the Nbs (Figure 3F; STAR Methods). Here, we used the transpeptidase enzyme sortase to attach peptide-linked 6-carboxyfluorescein (FAM) to the C terminus of the Nbs (STAR Methods). In this case, all Nbs clearly showed binding to the living trypanosomes (Figure 3F). To buttress the positive binding result for $NB19_{VSG2}$ by a third independent experiment, we also exposed living trypanosomes to the Nbs, thoroughly washed the cells, and then probed them by western blot (Figure 3G). All of the Nbs, including $NB19_{VSG2}$, were shown to have bound, whereas an irrelevant Nb raised to the *Helicobacter pylori* BabA antigen did not bind VSG2-expressing trypanosomes.

Probing Nb-VSG2 interactions

Nb-VSG2 interactions were also examined by using isothermal titration calorimetry (ITC, Figures S3A and S3B). These experiments revealed that while most Nbs bound with sub-micromolar affinity, $NB11_{VSG2}$ stood apart with a picomolar binding constant that is more than 10-fold stronger than any of the others (Figure S3B), most likely due to its ~30% larger contact surface.

To further examine the interactions of the Nbs with VSG2, we created mutations in the consensus site of CDR3 of $NB11_{VSG2}$ and two critical contacts to VSG2 from $NB19_{VSG2}$ (Figure 4). We focused on these two because $NB11_{VSG2}$ possesses a highly similar consensus binding site to $NB9_{VSG2}$ and $NB14_{VSG2}$, whereas $NB19_{VSG2}$ differs in the binding location and in sequence to the others. The alteration of these important contacts led to a disruption of binding to VSG2 as assayed by gel filtration chromatography. In particular, even single loss-of-contact mutations to the $NB19_{VSG2}$ interface completely disrupted

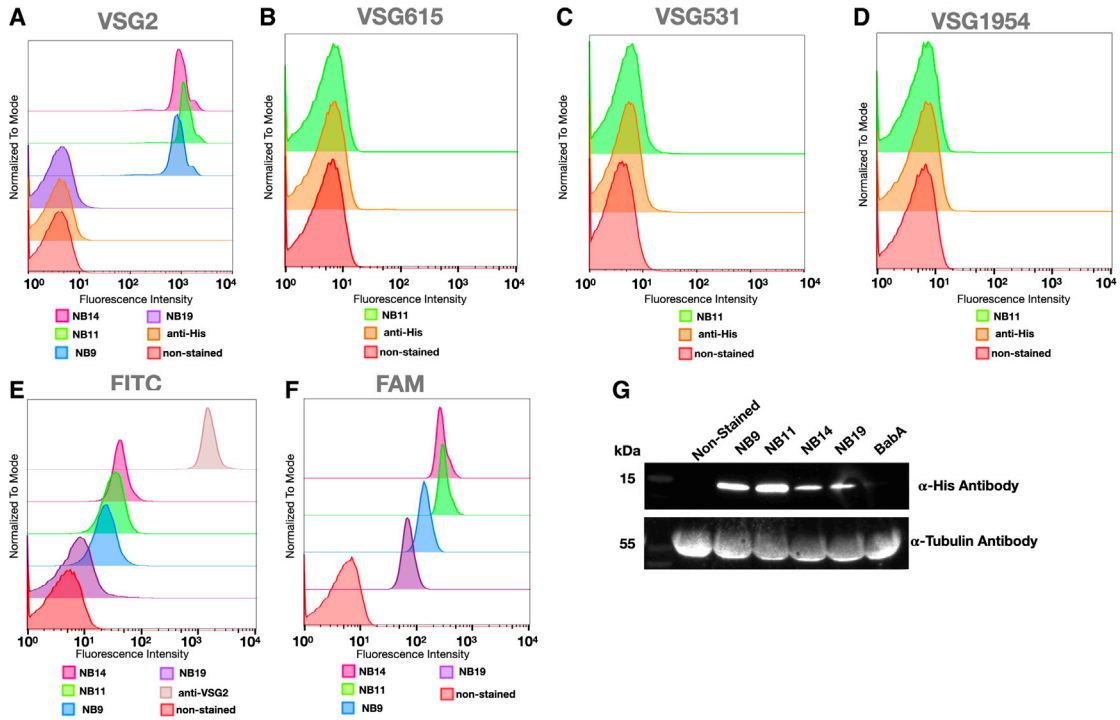

Figure 3. Binding assays of Nbs to live trypanosomes

Different VSG-expressing *T. brucei* samples were incubated with various Nbs and visualized in different ways by FACS.

(A) VSG2-expressing bloodstream form (BSF) trypanosomes were incubated with C-terminally His-tagged Nbs and visualized using an anti-His antibody.

(B) VSG615-expressing BSF trypanosomes (expressing a metacyclic VSG) were incubated with C-terminally His-tagged Nbs and visualized using an anti-His antibody.

(C) VSG531-expressing BSF trypanosomes were incubated with C-terminally His-tagged Nbs and visualized using an anti-His antibody.

(D) VSG1954-expressing BSF trypanosomes (expressing a metacyclic VSG) were incubated with C-terminally His-tagged Nbs and visualized using an anti-His antibody.

(E) VSG2-expressing BSF trypanosomes were incubated with FITC-labeled Nbs and visualized through the fluorochrome's emission.

(F) VSG2-expressing BSF trypanosomes were incubated with Nbs sortagged with FAM and visualized through the fluorochrome's emission.

(G) VSG2-expressing BSF trypanosomes were incubated with C-terminally His-tagged Nbs, washed thoroughly, run on an SDS-PAGE gel, and probed with an anti-His antibody. An irrelevant Nb (BabA, raised to a protein from *H. pylori*) was used as a negative control. The same cells were probed with an anti-tubulin antibody to provide a gel-loading standard.

binding, whereas it required a triple mutant in $NB11_{VSG2}$ ($NB11_{mut}$) to abrogate complex formation, suggesting that this complex was more stable (Figure 4). To assess whether this disruption of binding observed *in vitro* was observable *in vivo*, we tested the $NB11_{mut}$ on live parasites and assayed the results by FACS using an anti-His monoclonal antibody as in Figure 3. Consistent with the gel filtration experiments, no binding of the $NB11_{mut}$ could be detected to live cells (Figures S3C and S3D).

Nbs against VSG2 reduce coat mobility, cause stiffening of the cell body, and stall parasite motion

As previous reports had shown that VSG-targeting Nbs could kill trypanosomes following a rapid interference with trypanosome movement (Stijlemans et al., 2011), VSG2-expressing wild-type cells were treated with saturating amounts of the four Nbs to assess cell viability. Only treatment with $NB11_{VSG2}$ resulted in substantial cell death after 5 h of treatment (Figure 5A, left graph; Figure S4A; Table S3A) as assayed via flow cytometry. Cell death was specific to VSG2-expressing cells with $NB11_{VSG2}$ treatment not affecting VSG6-expressing cells (Figure S4B; Table S3A). Likewise, cell death did not occur upon treatment of VSG2-expressing cells with the $NB11_{VSG2}$ triple mutant ($NB11_{mut}$) (Figure S4C; Table S3A). Increasing the amount of Nb employed to a 4- and 10-fold molar excess did not lead to a substantial increase in cell death for $NB9_{VSG2}$-, $NB14_{VSG2}$-, and $NB19_{VSG2}$-treated cells (Figure S4D; Table S3A). A closer analysis of $NB11_{VSG2}$-treated cells in hourly intervals during 8 h (Figure 5A, right graph; Figure S4E; Table S3B) showed that at least 80% of treated cells survived for one hour, with the proportion of dead cells increasing continuously up to 8 hours when only about 25% of cells remained alive (Figure 5A, right graph; Table S3B). The amount of $NB11_{VSG2}$ used had a critical impact on cell death (Figures S4E and S4F). A 1:1 molar ratio of Nb to VSG2 monomer was required and sufficient to cause cell death within 5 h of induction (consistent with previous reports [Caljon et al., 2012]) with a sharp rise in the number of dead cells observed between samples with a 0.9- and 1.1-fold excess, while higher Nb concentrations did not alter the kinetics of the cellular response, suggesting that the VSG coat had been saturated with Nb (Figure S4F). Based on these results, all further experiments were carried out with a saturating 1.7-fold

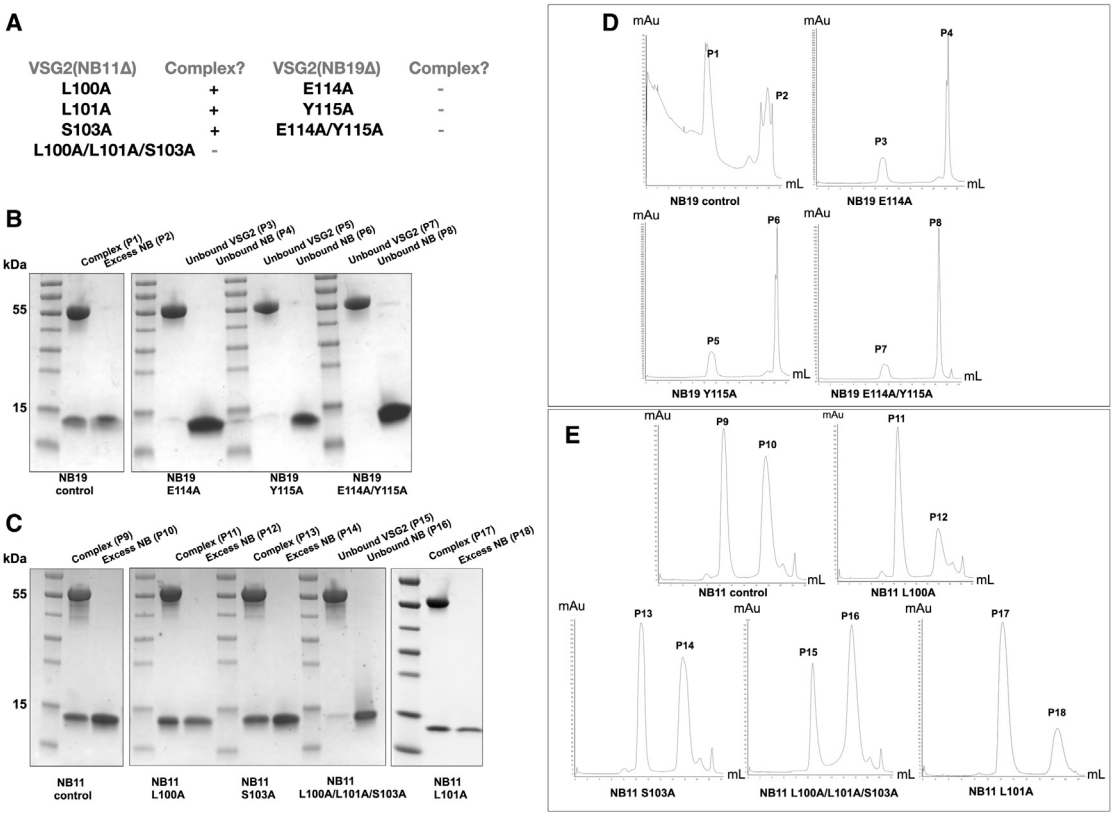

Figure 4. Mutations in the V-loop regions of Nbs inhibit complex formation with VSG2

(A) Overview of $NB11_{VSG2}$ and $NB19_{VSG2}$ mutants in relationship to their ability to bind VSG2.

(B and C) SDS-PAGE analysis of purified, mixed VSG2 and Nbs (wild-type and mutant $NB11_{VSG2}$ and $NB19_{VSG2}$) analyzed by gel filtration chromatography. Peak elution fractions are shown and numbered. VSG2 corresponds to the 55-kDa band and Nbs to the 15-kDa band. Gels were stained with Coomassie blue.

(D and E) FPLC chromatographs corresponding to the SDS-PAGE gels (B and C) with corresponding peak numbers from the SDS-PAGE gels shown. The y axis displays the UV_{280nm} absorbance, and the x axis displays the elution volume from the column.

excess of Nb to VSG monomer and within a 1-h window following Nb addition.

Ensemble measurements of cell motility were next performed upon treatment with all four Nbs and showed productive movement of trypanosomes to be hampered only following treatment with $NB11_{VSG2}$ (Figure 5B; Figure S5; Data S1). A plot of the swimming speed means, extracted from cell trajectories, at 5, 15, 25, and 35 min after addition of the respective Nbs showed a reduced mean velocity in $NB11_{VSG2}$-treated cells compared to $NB9_{VSG2}$-, $NB14_{VSG2}$-, and $NB19_{VSG2}$-treated cells, which behaved largely similar to untreated ones (Figure 5B, left panel). A similar plot using the extracted track displacement lengths per second also showed smaller values in $NB11_{VSG2}$-treated cells with a narrower range of distribution (Figure 5B, right panel). A closer analysis of cells following $NB11_{VSG2}$ treatment showed that while at 5 min after addition the swimming behavior of the parasites remained largely uninfluenced, with individual cells actively swimming and changing direction, from 15 min onward, cell movement was clearly affected as trajectories became shorter and mostly unidirectional (Figures 5C; Figure S5C). A closer inspection of these trajectories suggested that the parasites were not motionless, but that translocation was largely due to drift in the sample, which is unavoidable in recordings of this duration. To analyze this further, high-speed videos of treated and untreated individual cells (Figure 5D; Video S1) were acquired. Although Nb-treated parasites were unable to swim productively, the flagellar wave initiated as normal at the tip of the flagellum, but did not progress along the whole cell body, so that the typical cellular waveform could not be observed (Bargul et al., 2016). Thus, the parasites were partly paralyzed with increased stiffness and decreased ability to bend the cell body.

We next explored whether high-affinity Nb binding might affect VSG diffusion in the cell surface coat. Fluorescence recovery after photobleaching (FRAP) experiments were performed on immobilized cells with fluorescently labeled surface proteins. VSGs of untreated cells exhibited a median mobile fraction of 83% and diffusion coefficient of 0.020 $\mu m^2/s$. Addition of the Nb resulted in a marked reduction of the median mobile fraction to 11% with the diffusion coefficient reduced to a median of 0.007 $\mu m^2/s$ (Figure 5E, left and right graph, respectively). Hence, binding of $NB11_{VSG2}$ to VSG2 on the cell surface significantly affected the mobility of the protein in the cell surface coat.

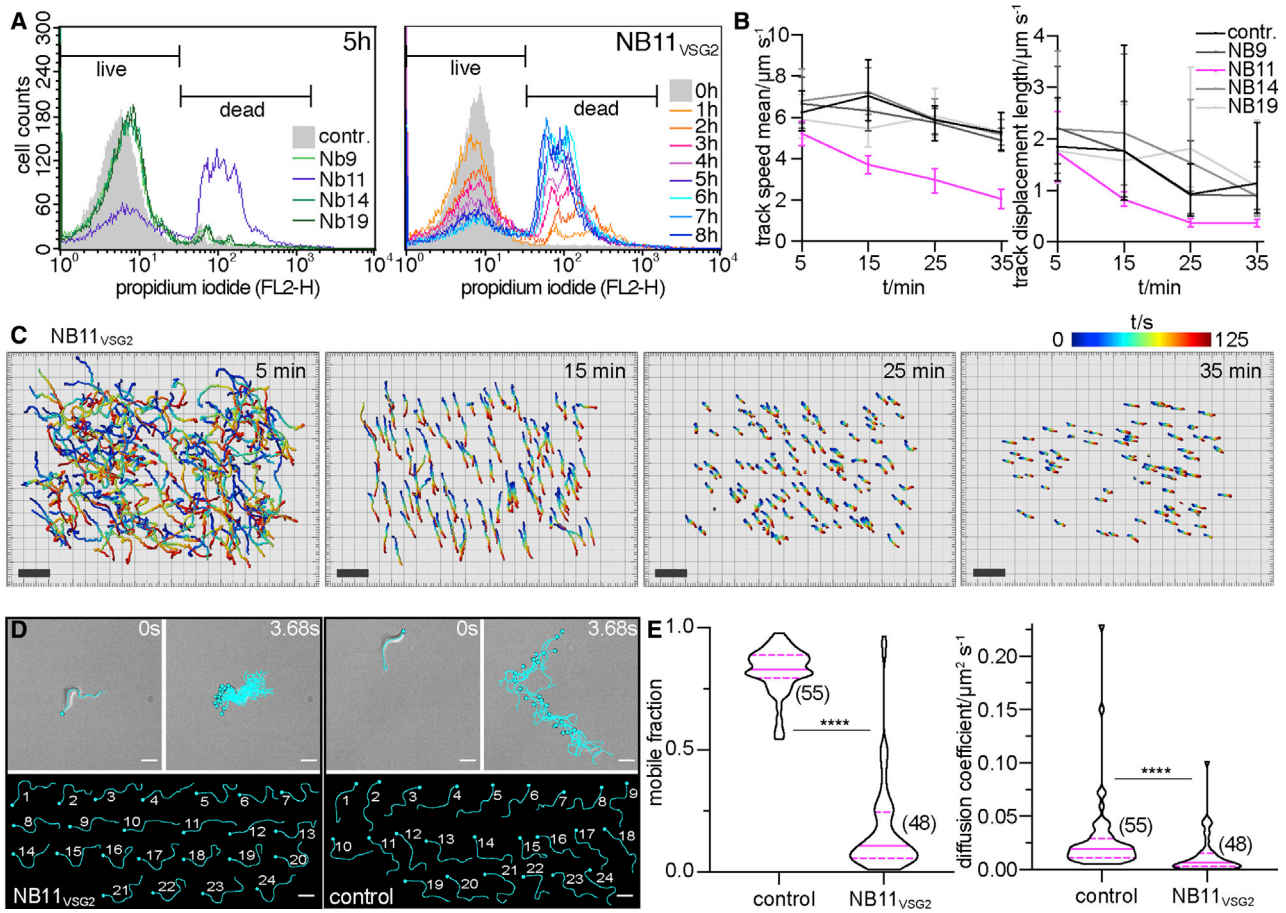

Figure 5. Nbs reduce VSG mobility, paralyze, and kill trypanosomes

(A–E) VSG2-expressing cells were treated with a 1.7-fold molar excess of Nb to VSG monomer.

(A) Flow cytometry analysis to determine the extent of cell death upon treatment with VSG2 targeting Nbs $NB9_{VSG2}$, $NB11_{VSG2}$, $NB14_{VSG2}$, and $NB19_{VSG2}$. Only treatment with $NB11_{VSG2}$ for 5 h resulted in large-scale cell death (left graph). Analysis of $NB11_{VSG2}$-treated cells in hourly intervals during 8 h showed a progression in the amount of dead cells observed, with most cells still alive at the 1 h time point. Propidium iodide was used as a dead cell marker. Each histogram is based on 25,000 gated events.

(B) Analysis of the swimming behavior following treatment with $NB9_{VSG2}$, $NB11_{VSG2}$, $NB14_{VSG2}$, and $NB19_{VSG2}$. Comparisons are shown of velocities (track speed mean) (left) and track displacement lengths per second (right) of untreated cells and cells treated with the four different Nbs. Data were extracted from trajectories shown in Figure S5 (median with bars representing the 25th and 75th percentile of data points; see Data S1 for scatter dot plots of the data). Both velocity and track displacement are clearly most affected upon treatment with $NB11_{VSG2}$.

(C) Cell trajectories of $NB11_{VSG2}$-treated cells at 5, 15, 25, and 35 min after addition. The Nb affects cell motility after 15 min of treatment. Individual cells in a population were tracked for 125 s at each shown time point after addition of $NB11_{VSG2}$ and analyzed using the Imaris x64 software (Oxford Instruments). Cells close to the border of the imaging region were removed by filtering to simplify the images shown (see Figure S5C for trajectories of complete dataset). Trajectories are color coded blue (t = 0 s) to red (t = 125 s). Scale bars, 100 µm.

(D) Single-cell analysis of the movement of an $NB11_{VSG2}$-treated (left panel) and an untreated trypanosome (right panel). The upper left image of each panel shows the first frame of a 920-frame-containing video (see Video S1) with the posterior of the cell marked by a cyan colored circle and the cell shape delineated by a longitudinal cyan colored line through the center of the cell. The upper right image of each panel shows the last frame of the video. To visualize cell movement from frame 1 to frame 920, the posterior and the cell shape are marked in the figure for cells in every 40th frame of the video. Whereas the flagellar beat generates a propulsive force in wild-type (WT) cells, the Nb-treated cells initiate beats without the generation of a propulsive force. The lower images in both panels show the same traces displayed individually to show more clearly differences in cell shape and orientation. Scale bars, 5 µm.

(E) The effect of Nb binding on VSG diffusion was analyzed by fluorescence recovery after photobleaching (FRAP) experiments on immobilized trypanosomes that were surface labeled with ATTO 488. Untreated (control) and $NB11_{VSG2}$-treated cells were analyzed (n in brackets). Violin plots show the frequency distribution of the mobile fractions (left) and the diffusion coefficient (right) of the VSG in control and $NB11_{VSG2}$-treated cells (median, solid magenta lines; 25th and 75th percentile, dashed magenta lines). There was a remarkable reduction in mobile fraction of treated cells (median of 11%) compared to that of untreated cells (median of 83%). The median diffusion coefficient of mobile VSGs following treatment with $NB11_{VSG2}$ was reduced to 0.007 $\mu m^2/s$ from 0.019 $\mu m^2/s$ for untreated cells. p values from an unpaired, two-tailed Mann-Whitney test (**** = $p < 0.0001$) are shown in both graphs.

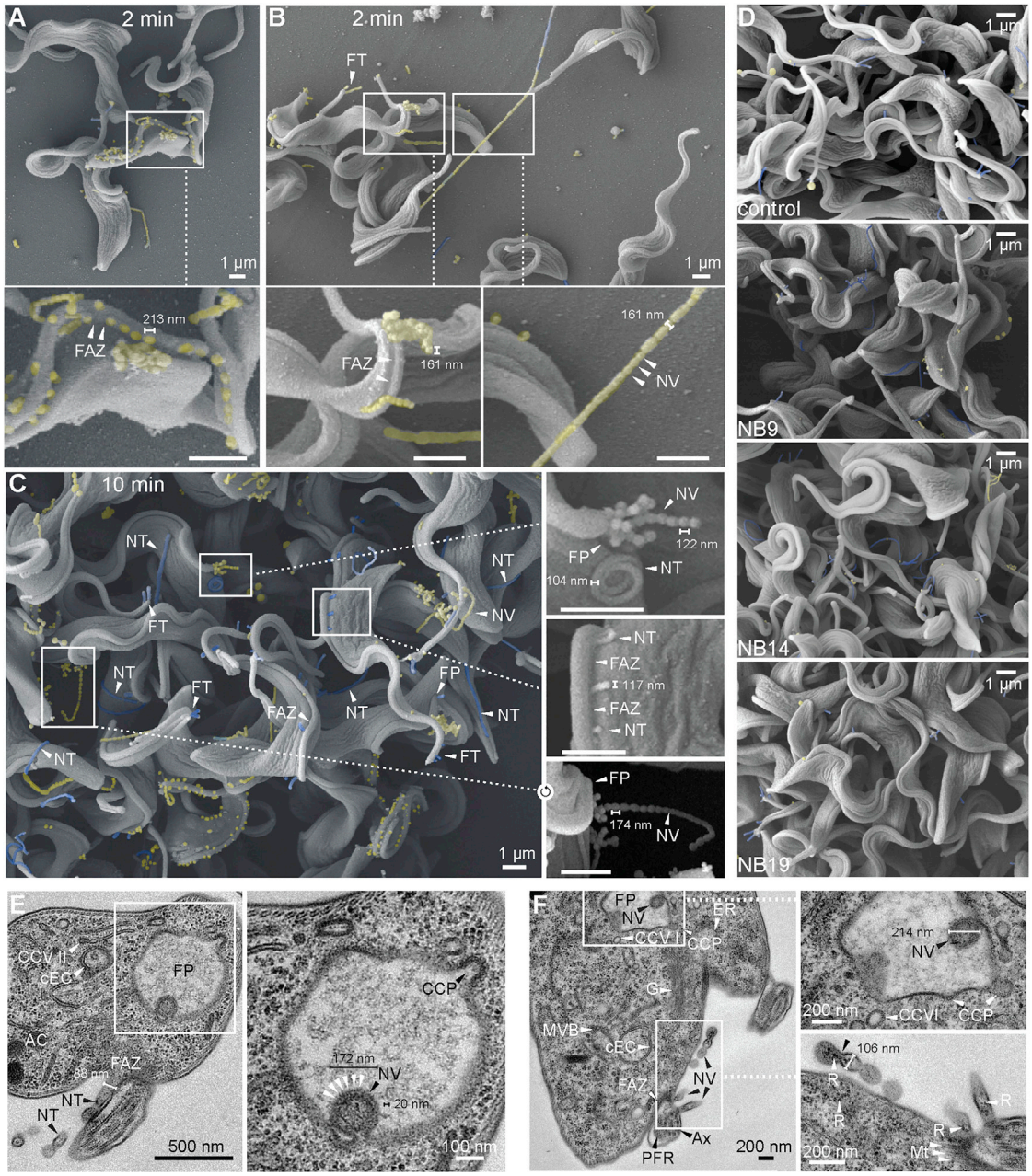

Figure 6. Nb treatment triggers formation of nanovesicles and nanotubes

(A–D) Scanning electron micrographs of VSG2-expressing trypanosomes treated with a 1.7-fold molar excess of anti-VSG2 Nbs compared to VSG monomer present. FAZ, flagellar attachment zone; FP, flagellar pocket; FT, flagellar tip; NT, nanotube; NV, nanovesicle; PP, posterior pole.

(A and B) Cells treated for only 2 min with $NB11_{VSG2}$ displayed NVs (yellow) as well as some chains of NVs (yellow) with diameters of around 200 nm. NT-like structures (blue) of slightly smaller diameter and lengths exceeding 1 μm could also be observed. All structures emanated from around the FAZ, FT, and PP.

(C) Cells treated for 10 min with $NB11_{VSG2}$ show an increased and roughly equal abundance of both NVs and NTs, suggesting them to be independent structures.

(D) Some NVs and short NTs could also be observed on individual untreated cells (control) but with a much lower incidence. $NB19_{VSG2}$-treated cells behaved largely like untreated cells whereas $NB9_{VSG2}$- and $NB14_{VSG2}$-treated cells did display an increased amount and length of NTs compared to the control cells. The abundance and extent, however, remained well below that found in $NB11_{VSG2}$-treated cells.

(E and F) TEM images of chemically fixed VSG2-expressing cells treated with a 1.7-fold molar excess of $NB11_{VSG2}$ compared to VSG2 monomer present. AC, acidocalcisome; Ax, axoneme; CCP, clathrin-coated pit; CCVI, clathrin-coated vesicle I; CCVII, clathrin-coated vesicle II; cEC, circular exocytic carrier; ER, endoplasmic reticulum; FAZ, flagellar attachment zone; FP, flagellar pocket; G, Golgi; Mt, mitochondrion; MVB, multivesicular body; NV, nanovesicle; NT, nanotube; PFR, paraflagellar rod; R, ribosome.

(legend continued on next page)

$NB11_{VSG2}$ induces the formation of nanovesicles and nanotubes on the trypanosome surface

Interestingly, scanning electron microscopy (SEM) of $NB11_{VSG2}$-treated VSG2-expressing cells revealed the formation of nanovesicles and nanotube-like structures as early as 2 min following addition of the Nb (Figures 6A and 6B). Initially, nanovesicles of around 200-nm diameter originated mainly from the flagellum attachment zone (FAZ), the flagellar tip (FT), and the posterior pole (PP) of the cell (Figures 6A and 6B; Figure S6A, middle and lower inset). In some parasites, the nanovesicles had formed vesicle chains (Figure 6B). In addition to these nanovesicles and vesicle chains, nanotubes of slightly smaller diameter, which could be more than 1 μm in length, appeared perpendicular to the FAZ (Figure S6A, upper inset). In the vast majority of cells, nanovesicles and/or nanotubes had been formed after 2 min, while after 5 min all parasites revealed this phenotype. Vesicles appeared on both sides of the FAZ and frequently at the origin of the flagellum, the FP (Figures S6B and S6C). Likewise, nanotubes were present in the vicinity of the FP (Figure S6C, left inset). Vesicles in close proximity to the FP tended to be larger (275 nm) than those appearing at the FAZ (150–180 nm). In some trypanosomes, the nanovesicles appearing alongside the FAZ seemed to fuse (Figure S6C, right inset) or to redistribute toward the flagellar membrane. However, after 10 min of Nb incubation, nanovesicles and nanotubes were still present with roughly the same abundance and with very little indication of a transition of nanovesicular chains to nanotubes, suggesting that both structures form independently (Figure 6C). After 15 min, the number of budding nanovesicles had decreased, and the nanotubes were greatly elongated, thereby apparently forming bridges between parasites. Some of the tubes seemed to be under tension (Figure S6D), while others formed catenated structures.

Occasionally, smaller nanotubes or nanovesicles appeared to branch off the main tube (Figure S6D, lower inset). The fact that most of the 10s of micrometer-long tubes were intact, without showing breakpoints, suggests that they are mechanically rather robust. This can be seen when tubes bend around trypanosomes (Figure S6D, middle inset). A closer inspection of the apparent network built from nanotubes revealed that most intersections in fact are crossings of two tubes without fusion (Figure S7A, upper inset), while other intersections seemed to represent true membrane fusion (Figure S7A, lower inset). The presence in nanotubes of nodes of similar size as nanovesicles is first seen after 20 min (Figure S7A, middle inset). The endpoint of our observation window was 25 min, when the nanotubes had formed concatenated or branched networks that are very difficult to trace by SEM (Figure S7B). However, it seems noteworthy that at this time point nanovesicles also emanated from the same trypanosome membrane areas as after 2 min of Nb incubation, namely along the FAZ, at the PP and at the FT (Figure S7B). Low-magnification overview images spanning the entire time course highlighting the extent of nanotube formation are shown in Figure S8A. Interestingly, when we looked at control parasites that had undergone the same experimental procedure, but without exposure to the Nb, we occasionally also observed nanovesicle formation at the FAZ, the FT, and the FP. Despite most trypanosomes displaying no or few nanovesicles (Figure 6D, control; Figure S7C, 25 min), short nanovesicular chains could be observed in some parasites (Figure 6D; Figure S7C, 10 min). Cells treated with $NB19_{VSG2}$ looked comparable to control cells, while cells treated with $NB9_{VSG2}$ and $NB14_{VSG2}$ showed an increased amount of nanotubes that were, however, not present in all cells and not as pronounced as in $NB11_{VSG2}$-treated cells (Figure 6D). A 2-fold reduction in $NB11_{VSG2}$ concentration used led to a decreased formation of nanotubes and nanovesicles (Figure S8B). Both $NB11_{VSG2}$ triple mutant ($NB11_{mut}$)-treated VSG2-expressing cells and $NB11_{VSG2}$-treated VSG6-expressing cells were indistinguishable from untreated control cells (Figure S8B). Importantly, the fact that nanovesicles and nanotubes were also formed in control cells suggests that this is a biologically relevant process that can be triggered in a spectacular manner by epitope-specific anti-VSG Nbs.

Nanovesicles and nanotubes are coated with VSGs and bud from the cell surface

Ultra-thin sections of trypanosomes, treated with Nb for 15 min, were prepared for transmission electron microscopy (TEM). The micrographs revealed an intracellular architecture that was indistinguishable from that found in non-treated parasites. Figure S9A shows perfect preservation of FP structure, including the tight junction at the FP collar, the FP matrix, and the VSG coat. Frequently, clathrin-coated pits were visible, indicating that the endocytosis machinery was at least structurally not impaired. Circular and flat endosomal cisternae were present, as well as class 2 clathrin-coated vesicles (CCV IIs), which are essential for cargo transport to late endosomes (Figure 6E) (Grünfelder et al., 2003). Likewise, mitochondrion, nucleus, endoplasmic reticulum, acidocalcisomes, glycosomes, Golgi, and the subpellicular microtubule corset did not show any significant alterations (Figure 6F; Figure S9B). Hence, 15 min after incubation with Nbs, the parasite's intracellular architecture was not impaired. Nevertheless, just as in SEM preparations, nanovesicles and nanotubes were readily observable in these TEM samples. These vesicles were covered with an electron-dense layer characteristic of the trypanosome's VSG surface coat, which was confirmed by immunofluorescence analysis (Figure S9G).

Interestingly, nanovesicles were found to be budding into the FP. Figure 6E shows a perfectly spherical budding vesicle that is decorated with evenly spaced structures. The inner diameter of this vesicle is 100 nm, and the outer structures have a size of about 20 nm, which is similar to the size of membrane-embedded VSGs. Note that a clathrin-coated pit is being formed at the same FP. Interestingly, the same cell is shedding

(E) Concomitant formation of a NV in the FP and a NT from the proximity of the FAZ. The formation of a clathrin-coated pit in the FP is also apparent and suggests the endocytic pathway to be functional. The budding NV has approximately 20-nm-thick structures coating the outer membrane consistent with the length of VSG molecules.

(F) Concomitant formation of a NV in the FP and NTs from the proximity of the FAZ. NVs can form chains with continuous content and contain electron-dense particles that resemble ribosomes found in the cytoplasm.

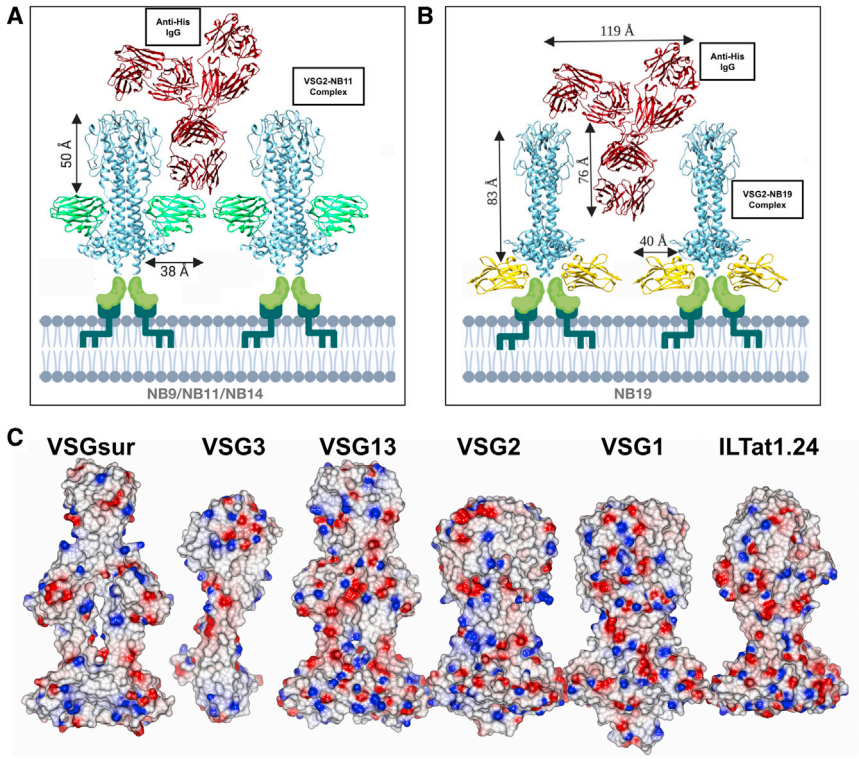

Figure 7. Nbs gauge VSG accessibility

(A and B) Schematics of the interaction of an anti-His monoclonal IgG antibody with the VSG coat during FACS experiments. The trypanosome membrane is shown at the bottom with idealized lipids into which the (dark green) GPI anchor of the C-terminal domain (medium green) inserts. Above that is a ribbon diagram drawing of a VSG2 dimer (cyan) with a bound Nb ($NB9_{VSG2}$, $NB11_{VSG2}$, $NB14_{VSG2}$) superimposed in light green (A) or $NB19_{VSG2}$ (gold) (B). The IgG is shown as a ribbon diagram colored red (PDB: 5DK3).

(C) Crystal structures of VSGs drawn as molecular surfaces colored by relative electrostatic potential (blue is positive/basic, red is negative/acidic, and white is neutral). RCSB PDB IDs for models used are ILTat1.24 (PDB: 2VSG), VSG1 (PDB: 5LY9), VSG2 (PDB: 1VSG), VSG13 (PDB: 6Z8H), VSG3 (PDB: 6ELC), and VSGsur (PDB: 6Z7A). Molecular graphics software used included Chimera (Pettersen et al., 2004), CCP4mg (McNicholas et al., 2011), and BioRender Pro.

nanotubes at the flagellar attachment zone. These are smaller in diameter than the FP-derived nanovesicles. From the micrographs, it is not clear how the nanovesicles exit the FP, as the tight junction and FP collar are intact (Figure S9B). Figure 6F shows another example of concomitant formation of large nanovesicles within the FP and nanovesicles/nanotubes at the flagellar attachment zone. These structures were probably the nanovesicular chains observed in SEM. Interestingly, the TEM images show that the "vesicles" were not always fully separated by membrane but had continuous content (Figure 6F, lower inset). In all of these vesicles, electron-dense particles were detected, which were identical with the cytoplasmic ribosomes in size and form (Figure 6F, lower inset). As the flagellum is free of ribosomes, the segmented nanotubes and free nanovesicles likely originate from the pellicular plasma membrane and not from the flagellum (Figure S9D). With ribosomes distributed in the cytoplasm, incorporation into the budding structures will inevitably occur. In contrast, the smooth and long nanotubes observed with SEM after 15 min of treatment could well originate from the flagellar membrane, as shown in Figure S9C. In this cell, multiple tubes bud from one flagellum. These are also covered by a VSG coat, but do not contain ribosome-like structures. The shedding of the smooth nanotubes must involve significant mechanical forces, as is suggested by marked membrane deformations, both on the flagellar side and on the nanotubes (Figure S9C, white arrows). In rare occasions, a nanotube branchpoint was observed (Figure S9E), but it remains unclear how these branches can form. Figure S9F shows that the tubes can be bent and deformed, which is in agreement with observations made in SEM micrographs.

DISCUSSION

Our experimental results confirm that the antigenic surface of the VSGs extends well beyond the upper surfaces of these molecules (Figure 7A). Such conclusions are consistent with the observations that the VSGs possess molecular surfaces with relatively high sequence divergence as well as markedly divergent surface properties not only at the "top" of the NTD, but across the entire molecule (Figure 7B). That the much more highly conserved CTD would be difficult for antibodies to access (located more than 100 Å below the surface), as shown previously (Schwede et al., 2011) and in our study, is also in harmony with this model.

We identified one Nb ($NB11_{VSG2}$) that was highly efficient in immobilizing and ultimately killing cells, a marked motility phenotype that is in accordance with published work (Stijlemans et al., 2011). In contrast, our work does not support the conclusion that this is due to impaired endocytosis and hence impaired energy supply. The onset of the motility phenotype was within minutes of Nb addition, and electron micrographs did not reveal any disruption in the endomembrane system, including the endosomes. What we observed was a marked reduction in cell body flexibility and increased stiffness of parts of the cell. This was not caused by paralysis of the flagellum, as it still initiated the beat that was, however, not propagated over the cell body. Hence, the trypanosomes did not swim anymore. We hypothesize that the phenotype observed could be related to the mobility and integrity of the surface coat.

We have previously shown that the VSG coat operates very close to a molecular crowding threshold, where a high lateral mobility is balanced with the highest possible density of the protein (Hartel et al., 2016). When the VSG density exceeds this threshold, translational diffusion in the surface coat is severely affected. This is exactly what might occur in the experiments reported herein. Binding of the Nb increases the hydrodynamic

radius of the VSG dimers, which results in a dramatic decrease in the mobile fraction. Thus, rotational and translational diffusion of the VSGs is confined by steric hindrance.

Thermodynamics in confinement would cause tension within the VSG coat due to pressure forces. If this were the case, there should be ultrastructural changes in surface topology of the trypanosomes. Indeed, we observed dramatic changes of the trypanosome cell surface in electron micrographs. We further hypothesize that the strong toxicity differences between the different Nbs are related to their relative affinities for VSG2. The only toxic Nb, $NB11_{VSG2}$, was shown by ITC to possess a 10-fold higher affinity to VSG2 (in the picomolar range) as compared to the next closest Nb.

Membrane fission is essential for the life of all cells. Cytokinesis, the generation of organelles such as the mitochondrion, endoplasmic reticulum (ER), and Golgi, as well as endomembrane trafficking are processes that all depend on this type of membrane remodeling. Complex machineries involving many proteins that can form helical scaffolds or constricting rings, as well as shallow membrane insertions, are thought to control membrane fission (Snead et al., 2017; Campelo and Malhotra, 2012).

The nanovesicles and nanotubes observed in this work on the trypanosome cell surface did not show any structural features that differed from the plasma membrane. They were decorated with an electron-dense VSG layer, but no additional coats that could be involved in vesicle formation were detectable. This is not unexpected, as it is very unlikely that the parasites can sense the Nb addition, transduce this information, and actively secrete a putative extracellular fission-promoting machinery, all within seconds. Thus, it is most probably not an active cellular process that drives nanovesicle and nanotube formation.

An attractive, alternative explanation for the phenotype would be protein-protein crowding. The addition of Nbs to the extremely dense VSG coat could, within seconds, raise the protein density on the cell surface above the molecular crowding threshold. In fact, we have shown that the lateral mobility of the VSG decreases rapidly after Nb addition, which supports this assumption. With the binding of Nbs, the mobility of the VSG becomes restricted and the coat is therefore under tension. Collisions of Nb-loaded VSGs will generate pressure (on one side of the plasma membrane). This behavior of a crowded membrane protein has been likened to that of compressed gas and it has been suggested to provide the pressure force required to initiate and complete membrane vesiculation and tubulation (Snead et al., 2017). Thus, Nb-mediated protein crowding could provide the energy required for membrane fission. No cellular machineries would be required to overcome the energy barrier. Membrane fission by protein-protein crowding has been observed before, albeit only in artificial systems and is supported by modeling approaches (Derganc and Čopič, 2016; Snead et al., 2017).

The fact that we find nanotubes and nanovesicles also in untreated cells, albeit only occasionally, suggests that, at least in trypanosomes, protein crowding-mediated extracellular vesiculation could be a biologically relevant process. We surmise that by using this passive, density-controlled process, the parasites can adjust the VSG coat density, e.g., during cell division or VSG switching.

Especially at early time points after addition of Nbs, vesicle chains of increasing length were observed. TEM images showed that the chains were not always composed of separated vesicles but were often segmented, continuous volumes. There are few reports on vesicle chains in biology. Outer membrane vesicle chains have been reported in *Myxococcus xanthus* (Remis et al., 2014), and biopearling has been observed in a marine flavobacterium (Fischer et al., 2019). However, the mechanisms underlying vesicle chain formation have not been studied. As segmented membrane volumes are detectable already after 2 min in Nb-treated trypanosomes, we surmise that counteracting mechanical forces interrupt full fission of nanovesicles. The segmented vesicle chains mainly appear at the FAZ and the FP. These regions continuously experience the forces exerted by the flagellar beat. It is tempting to speculate that the flagellar force causes interruption of fission events. In this way, the continuous beat of the flagellum would produce segments of very similar size. After about 15 min of Nb treatment, the vesicle chains disappear. This is the time point when the propagation of the flagellar beat is impaired, probably due to membrane tension caused by loss of membrane through vesiculation. Thus, the force producing the segmented membrane volumes decreases, resulting in a shift to tubulation. Importantly, note that fusion of nanotubes to neighboring parasites has not been observed, suggesting that cell-cell communication via membrane bridges is not occurring.

In summary, the fast onset of membrane fission at "free" membrane compartments could be explained by membrane tubulation through protein-protein crowding on the trypanosome cell surface. Are the nanovesicles in fact exosomes or ectosomes (extracellular vesicles [EVs])? Exosomes are produced by multivesicular bodies and secreted by exocytosis. This has previously been observed in fly-stage *T. brucei* procyclic forms (Eliaz et al., 2017). Since we did not find any changes in the endomembrane architecture, the vesicles formed after Nb treatment are likely not exosomes. The formation of extracellular vesicles in trypanosomes was first reported in 2016 (Szempruch et al., 2016). In contrast to our data, this work revealed that EVs were generated by vesiculation of nanotubes that are highly fusogenic and originate from the flagellar membrane. Thus, despite morphological similarities, the nanovesicles and nanotubes observed in the present study are neither exosomes nor ectosomes, but rather the product of membrane fission through protein-protein crowding.

Limitations of the study

In this study we have generated Nbs against VSG2, one member of the large family of VSGs found in *T. brucei*, and characterized their binding properties, such as binding location and affinity to VSG2. One of these Nbs, $NB11_{VSG2}$, showed a higher binding affinity to VSG2 than the others despite binding to the same location as $NB9_{VSG2}$ and $NB14_{VSG2}$. Its ~30% larger contact surface is the most likely explanation for this difference. Further mutagenesis studies could provide solid evidence. Furthermore, the high-affinity binding $NB11_{VSG2}$ disrupted cell motility and the free diffusion of the VSG coat, specifically in VSG2-expressing cells, culminating in cell death. Analysis of $NB11_{VSG2}$-treated cells via both SEM and TEM revealed the formation and

shedding of nanovesicles and nanotubes from specific regions of the parasites, namely the flagellar attachment zone, the posterior of the cell, the area of the FP, and the tip of the flagellum. The data presented are consistent with the concept that high-affinity binding of the Nb leads to protein crowding, which in turn mediates membrane shedding. However, much remains to be learned about the details of this shedding process. What is the actual occupancy of Nb in the surface coat when shedding occurs? How is the mobility of individual VSGs affected? What forces are required to lead to membrane budding? What dictates whether nanotubes or nanovesicles are formed? More broadly, how often is molecular crowding a stimulus to membrane fission in biology? All of these questions have only arisen as a result of the study presented here, and addressing these in the future seems feasible.

STAR★METHODS

Detailed methods are provided in the online version of this paper and include the following:

- KEY RESOURCES TABLE
- RESOURCE AVAILABILITY
  - Lead contact
  - Materials availability
  - Data and code availability
- EXPERIMENTAL MODEL AND SUBJECT DETAILS
- METHOD DETAILS
  - Production of nanobodies
  - Production of nanobody mutants
  - Production of sortaggable nanobodies
  - Synthesis of a His-tagged VSG2-irrelevant nanobody (NB-ER19)
  - Purification of VSG2
  - Purification and crystallization of VSG2-nanobody complexes
  - Structure determination of VSG2-nanobody complexes
  - Cloning, expression, purification, and sortagging of camelid VHH-IgG2 heavy chain antibodies
  - Sortagging of VSG2 nanobodies
  - Flow cytometry analysis of heavy chain IgG2 binding to the native VSG2 coat on *T. brucei*
  - Flow cytometry analysis of nanobodies binding to the native VSG2 coat on *T. brucei*
  - Flow cytometry analysis of FAM-sortagged nanobodies binding to the native VSG2 coat on *T. brucei*
  - Flow cytometry analysis of $NB11_{VSG2}$ binding to different native VSG coats on *T. brucei*
  - Flow cytometry analysis of FITC-conjugated nanobodies binding to the native VSG2 coat on *T. brucei*
  - Western blot analysis
  - *T. brucei* culturing for motility and toxicity assays
  - Cell viability assay via flow cytometry
  - Tracking of individual cells in a population
  - High-speed microscopy of single cells
  - Fluorescence recovery after photobleaching (FRAP) experiments
  - Sample preparation for SEM
  - Chemical fixation and subsequent Epon embedding for TEM
  - High-pressure freezing and Epon embedding for TEM
  - Preparation of stained and contrasted sections for TEM analysis
  - Immunofluorescence assays
- QUANTIFICATION AND STATISTICAL ANALYSIS
  - Isothermal titration calorimetry
  - Flow cytometry analysis of mutated NB11 incubated to the native VSG2 coat on *T. brucei*

SUPPLEMENTAL INFORMATION

Supplemental information can be found online at https://doi.org/10.1016/j.celrep.2021.109923.

ACKNOWLEDGMENTS

We acknowledge synchrotron time at the Diamond Light Source (DLS, beamline i03, Neil Paterson) and at the Paul Scherrer Institut, Villingen, Switzerland (SLS, beamline PXIII, Vincent Olieric and colleagues). We thank Steve Schoonooghe, Ema Estevens Romão, and Gholamreza Hassanzadeh Ghassabeh of the Vlaams Instituut voor Biotechnologie (VIB) Nanobody Core facility for working closely with us to produce anti-VSG2 VHH antibodies and donating for experimental controls the antibody to *H. pylori* BabA. We thank Elisabeth Meyer-Natus (Würzburg) for technical assistance with electron microscopy sample preparation and data acquisition. We thank Tim Krüger (Würzburg) for assistance with microscopy and Susanne Fenz (Würzburg) for helpful discussions. We thank Jonas Wilhelm (MPI for Medical Research, Heidelberg) and Anna Svirina (DKFZ, Heidelberg) for technical assistance with ITC data collection and processing. M.E. is supported by DFG grants EN305, DFG-SPP1726, and DFG-GRK2157 and GIF grant I-473-416.13/2018. Work in the F.N.P. and C.E.S labs is funded by the Helmholtz Foundation.

AUTHOR CONTRIBUTIONS

C.E.S., F.N.P., M.E., and N.G.J. conceived, initiated, and coordinated the project. M.v.S. produced VSG2 for production of nanobodies. M.v.S. and A.H. produced and crystallized $NB11_{VSG2}$ and $NB14_{VSG2}$ complexes. A.H. produced and crystallized $NB9_{VSG2}$ and $NB19_{VSG2}$ complexes and all complexes for membrane studies (with M.v.S. also producing $NB11_{VSG2}$ and $NB14_{VSG2}$ for the latter), and collected the diffraction data and solved all structures. J.P.Z. aided in crystal preparation and beamline data collection. A.H. produced all protein material for the biological assays. H.H. and A.H. created sortaggable Nbs and the camelid heavy chain Ig2. H.H., M.v.S., and A.H performed anti-His FACS binding experiments. H.H. and A.H. produced the FAM and FITC FACS data on live *T. brucei*, while A.H. executed FACS experiments on non-VSG2 coats. A.H. performed all ITC experiments. L.H. performed all parasite movement and coat diffusion experiments. L.H. and K.B. performed electron microscopy and toxicity experiments. C.E.S., A.H., N.G.J., and M.E. wrote the manuscript. All authors discussed the data and approved the final manuscript.

DECLARATION OF INTERESTS

The authors declare no competing interests.

Received: March 15, 2021
Revised: August 6, 2021
Accepted: October 11, 2021
Published: November 2, 2021

REFERENCES

Adams, P.D., Afonine, P.V., Bunkóczi, G., Chen, V.B., Davis, I.W., Echols, N., Headd, J.J., Hung, L.W., Kapral, G.J., Grosse-Kunstleve, R.W., et al. (2010). PHENIX: A comprehensive Python-based system for macromolecular structure solution. Acta Crystallogr. D Biol. Crystallogr. *66*, 213–221.

Alsford, S., Kawahara, T., Glover, L., and Horn, D. (2005). Tagging a *T. brucei RRNA* locus improves stable transfection efficiency and circumvents inducible expression position effects. Mol. Biochem. Parasitol. *144*, 142–148.

Arbabi-Ghahroudi, M. (2017). Camelid single-domain antibodies: Historical perspective and future outlook. Front. Immunol. *8*, 1589.

Bangs, J.D. (2018). Evolution of antigenic variation in African trypanosomes: Variant surface glycoprotein expression, structure, and function. BioEssays *40*, e1800181.

Bargul, J.L., Jung, J., McOdimba, F.A., Omogo, C.O., Adung'a, V.O., Krüger, T., Masiga, D.K., and Engstler, M. (2016). Species-specific adaptations of trypanosome morphology and motility to the mammalian host. PLoS Pathog. *12*, e1005448.

Bartossek, T., Jones, N.G., Schäfer, C., Cvitković, M., Glogger, M., Mott, H.R., Kuper, J., Brennich, M., Carrington, M., Smith, A.S., et al. (2017). Structural basis for the shielding function of the dynamic trypanosome variant surface glycoprotein coat. Nat. Microbiol. *2*, 1523–1532.

Battye, T.G.G., Kontogiannis, L., Johnson, O., Powell, H.R., and Leslie, A.G.W. (2011). *iMOSFLM*: A new graphical interface for diffraction-image processing with *MOSFLM*. Acta Crystallogr. D Biol. Crystallogr. *67*, 271–281.

Borst, P. (2002). Antigenic variation and allelic exclusion. Cell *109*, 5–8.

Bülow, R., Overath, P., and Davoust, J. (1988). Rapid lateral diffusion of the variant surface glycoprotein in the coat of *Trypanosoma brucei*. Biochemistry *27*, 2384–2388.

Caljon, G., Stijlemans, B., Saerens, D., Van Den Abbeele, J., Muyldermans, S., Magez, S., and De Baetselier, P. (2012). Affinity is an important determinant of the anti-trypanosome activity of nanobodies. PLoS Negl. Trop. Dis. *6*, e1902.

Campelo, F., and Malhotra, V. (2012). Membrane fission: The biogenesis of transport carriers. Annu. Rev. Biochem. *81*, 407–427.

Collaborative Computational Project, Number 4 (1994). The CCP4 suite: Programs for protein crystallography. Acta Crystallogr. D Biol. Crystallogr. *50*, 760–763.

Cross, G.A.M. (1984). Release and purification of *Trypanosoma brucei* variant surface glycoprotein. J. Cell. Biochem. *24*, 79–90.

de Beer, T.A.P., Berka, K., Thornton, J.M., and Laskowski, R.A. (2014). PDBsum additions. Nucleic Acids Res. *42*, D292–D296.

de Marco, A. (2011). Biotechnological applications of recombinant single-domain antibody fragments. Microb. Cell Fact. *10*, 44.

Derganc, J., and Čopič, A. (2016). Membrane bending by protein crowding is affected by protein lateral confinement. Biochim. Biophys. Acta *1858*, 1152–1159.

Eliaz, D., Kannan, S., Shaked, H., Arvatz, G., Tkacz, I.D., Binder, L., Waldman Ben-Asher, H., Okalang, U., Chikne, V., Cohen-Chalamish, S., and Michaeli, S. (2017). Exosome secretion affects social motility in *Trypanosoma brucei*. PLoS Pathog. *13*, e1006245.

Emsley, P., Lohkamp, B., Scott, W.G., and Cowtan, K. (2010). Features and development of Coot. Acta Crystallogr. D Biol. Crystallogr. *66*, 486–501.

Engstler, M., Pfohl, T., Herminghaus, S., Boshart, M., Wiegertjes, G., Heddergott, N., and Overath, P. (2007). Hydrodynamic flow-mediated protein sorting on the cell surface of trypanosomes. Cell *131*, 505–515.

Engstler, M., Thilo, L., Weise, F., Grünfelder, C.G., Schwarz, H., Boshart, M., and Overath, P. (2004). Kinetics of endocytosis and recycling of the GPI-anchored variant surface glycoprotein in *Trypanosoma brucei*. J. Cell Sci. *117*, 1105–1115.

Fischer, T., Schorb, M., Reintjes, G., Kolovou, A., Santarella-Mellwig, R., Markert, S., Rhiel, E., Littmann, S., Becher, D., Schweder, T., et al. (2019). Biopearling of interconnected outer membrane vesicle chains by a marine flavobacterium. Appl. Environ. Microbiol. *85*, e00829-19.

Freymann, D., Down, J., Carrington, M., Roditi, I., Turner, M., and Wiley, D. (1990). 2.9 Å resolution structure of the N-terminal domain of a variant surface glycoprotein from *Trypanosoma brucei*. J. Mol. Biol. *216*, 141–160.

Grünfelder, C.G., Engstler, M., Weise, F., Schwarz, H., Stierhof, Y.-D., Morgan, G.W., Field, M.C., and Overath, P. (2003). Endocytosis of a glycosylphosphatidylinositol-anchored protein via clathrin-coated vesicles, sorting by default in endosomes, and exocytosis via RAB11-positive carriers. Mol. Biol. Cell *14*, 2029–2040.

Hartel, A.J.W., Glogger, M., Guigas, G., Jones, N.G., Fenz, S.F., Weiss, M., and Engstler, M. (2015). The molecular size of the extra-membrane domain influences the diffusion of the GPI-anchored VSG on the trypanosome plasma membrane. Sci. Rep. *5*, 10394.

Hartel, A.J., Glogger, M., Jones, N.G., Abuillan, W., Batram, C., Hermann, A., Fenz, S.F., Tanaka, M., and Engstler, M. (2016). N-glycosylation enables high lateral mobility of GPI-anchored proteins at a molecular crowding threshold. Nat. Commun. *7*, 12870.

Hirumi, H., and Hirumi, K. (1991). In vitro cultivation of *Trypanosoma congolense* bloodstream forms in the absence of feeder cell layers. Parasitology *102*, 225–236.

Horn, D. (2014). Antigenic variation in African trypanosomes. Mol. Biochem. Parasitol. *195*, 123–129.

McCoy, A.J., Grosse-Kunstleve, R.W., Adams, P.D., Winn, M.D., Storoni, L.C., and Read, R.J. (2007). Phaser crystallographic software. J. Appl. Cryst. *40*, 658–674.

McNicholas, S., Potterton, E., Wilson, K.S., and Noble, M.E.M. (2011). Presenting your structures: The CCP4mg molecular-graphics software. Acta Crystallogr. D Biol. Crystallogr. *67*, 386–394.

Moonens, K., Gideonsson, P., Subedi, S., Bugaytsova, J., Romaõ, E., Mendez, M., Nordén, J., Fallah, M., Rakhimova, L., Shevtsova, A., et al. (2016). Structural insights into polymorphic ABO glycan binding by *Helicobacter pylori*. Cell Host Microbe *19*, 55–66.

Mugnier, M.R., Stebbins, C.E., and Papavasiliou, F.N. (2016). Masters of disguise: Antigenic variation and the VSG coat in *Trypanosoma brucei*. PLoS Pathog. *12*, e1005784.

M. Mulisch and U. Welsch, eds. (2015). Romeis—Mikroskopische Technik (Springer).

Overath, P., Chaudhri, M., Steverding, D., and Ziegelbauer, K. (1994). Invariant surface proteins in bloodstream forms of *Trypanosoma brucei*. Parasitol. Today *10*, 53–58.

Pal, A., Hall, B.S., Jeffries, T.R., and Field, M.C. (2003). Rab5 and Rab11 mediate transferrin and anti-variant surface glycoprotein antibody recycling in *Trypanosoma brucei*. Biochem. J. *374*, 443–451.

Pettersen, E.F., Goddard, T.D., Huang, C.C., Couch, G.S., Greenblatt, D.M., Meng, E.C., and Ferrin, T.E. (2004). UCSF Chimera—A visualization system for exploratory research and analysis. J. Comput. Chem. *25*, 1605–1612.

Phair, R.D., Gorski, S.A., and Misteli, T. (2004). Measurement of dynamic protein binding to chromatin *in vivo*, using photobleaching microscopy. Methods Enzymol. *375*, 393–414.

Pinger, J., Chowdhury, S., and Papavasiliou, F.N. (2017). Variant surface glycoprotein density defines an immune evasion threshold for African trypanosomes undergoing antigenic variation. Nat. Commun. *8*, 828.

Radwanska, M., Vereecke, N., Deleeuw, V., Pinto, J., and Magez, S. (2018). Salivarian trypanosomosis: A review of parasites involved, their global distribution and their interaction with the innate and adaptive mammalian host immune system. Front. Immunol. *9*, 2253.

Remis, J.P., Wei, D., Gorur, A., Zemla, M., Haraga, J., Allen, S., Witkowska, H.E., Costerton, J.W., Berleman, J.E., and Auer, M. (2014). Bacterial social networks: Structure and composition of *Myxococcus xanthus* outer membrane vesicle chains. Environ. Microbiol. *16*, 598–610.

Rueden, C.T., Schindelin, J., Hiner, M.C., DeZonia, B.E., Walter, A.E., Arena, E.T., and Eliceiri, K.W. (2017). ImageJ2: ImageJ for the next generation of scientific image data. BMC Bioinformatics *18*, 529.

Schwede, A., Jones, N., Engstler, M., and Carrington, M. (2011). The VSG C-terminal domain is inaccessible to antibodies on live trypanosomes. Mol. Biochem. Parasitol. *175*, 201–204.

Schwede, A., Macleod, O.J., MacGregor, P., and Carrington, M. (2015). How does the VSG coat of bloodstream form African trypanosomes interact with external proteins? PLoS Pathog. *11*, e1005259.

Snead, W.T., Hayden, C.C., Gadok, A.K., Zhao, C., Lafer, E.M., Rangamani, P., and Stachowiak, J.C. (2017). Membrane fission by protein crowding. Proc. Natl. Acad. Sci. USA *114*, E3258–E3267.

Stijlemans, B., Conrath, K., Cortez-Retamozo, V., Van Xong, H., Wyns, L., Senter, P., Revets, H., De Baetselier, P., Muyldermans, S., and Magez, S. (2004). Efficient targeting of conserved cryptic epitopes of infectious agents by single domain antibodies. African trypanosomes as paradigm. J. Biol. Chem. *279*, 1256–1261.

Stijlemans, B., Caljon, G., Natesan, S.K.A., Saerens, D., Conrath, K., Pérez-Morga, D., Skepper, J.N., Nikolaou, A., Brys, L., Pays, E., et al. (2011). High affinity nanobodies against the *Trypanosome brucei* VSG are potent trypanolytic agents that block endocytosis. PLoS Pathog. *7*, e1002072.

Stijlemans, B., De Baetselier, P., Caljon, G., Van Den Abbeele, J., Van Ginderachter, J.A., and Magez, S. (2017). Nanobodies as tools to understand, diagnose, and treat African trypanosomiasis. Front. Immunol. *8*, 724.

Szempruch, A.J., Sykes, S.E., Kieft, R., Dennison, L., Becker, A.C., Gartrell, A., Martin, W.J., Nakayasu, E.S., Almeida, I.C., Hajduk, S.L., and Harrington, J.M. (2016). Extracellular vesicles from *Trypanosoma brucei* mediate virulence factor transfer and cause host anemia. Cell *164*, 246–257.

Vonrhein, C., Flensburg, C., Keller, P., Sharff, A., Smart, O., Paciorek, W., Womack, T., and Bricogne, G. (2011). Data processing and analysis with the *autoPROC* toolbox. Acta Crystallogr. D Biol. Crystallogr. *67*, 293–302.

Webster, P., Russo, D.C., and Black, S.J. (1990). The interaction of *Trypanosoma brucei* with antibodies to variant surface glycoproteins. J. Cell Sci. *96*, 249–255.

Winter, G., Lobley, C.M.C., and Prince, S.M. (2013). Decision making in *xia2*. Acta Crystallogr. D Biol. Crystallogr. *69*, 1260–1273.

STAR★METHODS

KEY RESOURCES TABLE

REAGENT or RESOURCE	SOURCE	IDENTIFIER
Antibodies		
Anti-6x-His	Abcam	ab1206; RRID: AB_298815
Anti-α-Tubulin	Abcam	ab0474; RRID: AB_2288001
Anti-Rabbit	Biorad	170-6515; RRID: AB_11125142
Rabbit anti-VSG221 (polyclonal serum)	raised against native VSG221 purified from *Trypanosoma brucei brucei* (own purification), custom made by BJ-Diagnostik Bio Science	Rb anti-VSG221, 14013, 1st bleed, 05.03.2014 (lab internal)
Goat anti-Rabbit Alexa Fluor 488	Invitrogen	A11008; RRID:AB_143165
Bacterial and virus strains		
WK6	ATCC	47078
DH5α	Thermo Fisher	18265017
Biological Samples	N/A	N/A
Chemicals, peptides, and recombinant proteins		
Tryptone	Sigma-Aldrich	91079-40-2
IPTG	Roth	2316.4
Glucose	ACROS	410950010
Trisma base	SIGMA	77-86-1
EDTA	Thermo Fisher	17892
Ni-NTA	QIAGEN	166017069
Sucrose	SIGMA	57-50-1
Imidazole	ROTH	X998.4
HMI-9	PAN Biotech	so-15701
FBS	GIBCO	2024-02
L-Cysteine	SERVA	190022
β-Mercaptoethanol	SIGMA	102039442
Yeast extract	GERBU	8013-01-2
Ampicillin	Sigma-Aldrich	BCBZ9179
Magnesium chloride	Merck	7786-30-3
HEPES	Roth	0195.3
Sodium chloride	Fisher Chemical	7647-14-5
Zinc chloride	Merck	7646-85-7
Q-Sepharose	GE Healthcare	17-0510-01
LysC Protease	NEB	10052276
Dipotassium phosphate trihydrate	SUPELCO	a1351199024
FreeStyle 293 Expression media	GIBCO	2085258
Monopotassium phosphate	SIGMA	7778-77-0
Sortase A	Internal production	N/A
AAGG-5-FAM	Biomatic	N/A
SDS	Panreac Applichem	7U014009
TBS	Merck	MFCD00132476
Tween-20	BIO RAD	1610781
Skimmed Milk Powder	SERVA	68514-61-4
Methylcellulose	Sigma-Aldrich	MO512

(*Continued on next page*)

Continued

REAGENT or RESOURCE	SOURCE	IDENTIFIER
Propidium iodide	Sigma-Aldrich	P4170
Glutaraldehyde	Merck	1.04239.0250
Disodium hydrogen phosphate	Applichem	A4732.1000
Acetone	Applichem	131007.1611
Gold-palladium	Baltic Praeparation	BP 2229
Cacodylate buffer	Roth	5169.2
Osmium tetroxide	Electron Microscopy Sciences	19130
Uranyl acetate	Merck	8473
Ethanol	Th. Geyer	2246.2500
Propylene oxide	Sigma-Aldrich	110205-2.5l
Epon 812	Serva	21045.02
Epon accelerator	Serva	36975.01
DDSA	Serva	20755.02
MNA	Serva	29452.03
Tannic Acid	Applichem	A3619.0250
Pioloform	Plano	R1275
Copper grids	Plano	G2500C
Lead (II) nitrate	Merck	1.07398.0100
tri-Sodium citrate dehydrate	Applichem	A2403.0500
Potassium chloride	Applichem	A3582.1000
BSA	Applichem	A1391.0100
Vectashield	Biozol	VEC-H-1000
DAPI	Applichem	A1001,0010
Magnesium sulfate	Serva	28311
Sodium dihydrogen phosphate	Applichem	A1373.1000
ATTO 488 NHS-ester	ATTO-TEC GmbH	AD488 31
Type A gelatin	Sigma-Aldrich	G18900-500G
Hellmanex	Hellma Analytics	9-307-011-4-507
PEG 1500	Sigma-Aldrich	225322-68-3
ADA	Sigma-Aldrich	10202164
Citrate	Sigma Aldrich	102206486
Ammonium sulfate	Sigma Aldrich	BCBX0350
Magnesium sulfate	Merck	7487-88-9
PEG 400	Merck	25322-66-3
LB Broth	SIGMA	102123542
Critical commercial assays		
FITC Conjugation Kit – Lightning	Abcam	ab102884
Pierce ECL	Thermo Fisher	32209
NEB HiFi DNA Assembly kit	New England Biolab	E5520S
Q5 High-Fidelity DNA Polymerase kit	New England Biolab	E0555S
BCA protein concentration kit	Pierce	23227
Deposited Data		
VSG2(NB9VSG2)	This Paper	7AQX
VSG2(NB11VSG2)	This Paper	7AQY
VSG2(NB14VSG2)	This Paper	7AQZ
VSG2(NB19VSG2)	This Paper	7AR0

(*Continued on next page*)

Continued

REAGENT or RESOURCE	SOURCE	IDENTIFIER
Experimental Models: Cell Lines		
Experimental models: Organisms/strains		
Trypanosoma brucei brucei 2T1	David Horn, University of Dundee	Alsford et al., 2005
Trypanosoma brucei brucei Lister 427, clone 221	George Cross, Rockefeller University	https://tryps.rockefeller.edu/DocumentsGlobal/lineage_Lister427.pdf
Oligonucleotides (shown 5′ to 3′)		
NB19_Y115A_rev	Sigma-Aldrich	N/A
TGGCCCCATGCCTCATACCACCCTGCA CTTTTAAGG		
NB19_Y115A_fwd	Sigma-Aldrich	N/A
TAT GAGGCATGGGGCCAGGGGACCCAGG		
NB19_E114A_Y115A_fwd	Sigma-Aldrich	N/A
GTGGTATGCGGCCTGGGGCCAGG		
NB19_E114A_Y115A_rev	Sigma-Aldrich	N/A
CCTGCACTTTTAAGGGCCATGTCG		
NB9/11/14_universal_fwd	Sigma-Aldrich	N/A
GATGTGCAGCTGCAGGAG TCTGGRGGAGG		
NB9/11/14_universal_rev	Sigma-Aldrich	N/A
CTAGTGCGGCCGCTGAGG AGACGGT GACCTGGGT		
NB19_fwd	Sigma-Aldrich	N/A
TCCCTGGACCCTGGCGGAACCAGCC		
NB19_rev	Sigma-Aldrich	N/A
GGCTGGTTCCGCCAGGGTCCAGGGA		
cHC-Cam-IgG2_fwd	Sigma-Aldrich	N/A
GGTCACCGTCTCCTCAGAGCCAA AGATTCCGCAG		
cHC-Cam-IgG2_rev	Sigma-Aldrich	N/A
CCTGCAGCTGCACCTGACACTGAACCCCCTTCA		
pHen6C-ER19_fwd	Sigma-Aldrich	N/A
GGAAAACCCTGGCGTTACCCAA		
pHen6C-ER19_rev	Sigma-Aldrich	N/A
CAATCCAGCGGCTGCCGTAG		
NB19_Y114A_fwd	Sigma-Aldrich	N/A
TGCATACTGGGGCCAGGGGACCCAGGTCA		
NB19_Y114A_rev	Sigma-Aldrich	N/A
CTGGCCCCAGTATGCATACCACCCTGCAC TTTTAAG		
NB11_L100A_fwd	Sigma-Aldrich	N/A
GTAACGACTACTACCTAAGGCCTTCGCCG CACAGTAATAC		
NB11_L100A_rev	Sigma-Aldrich	N/A
GTATTACTGTGCGGCGAAGGCCTTAAGTA GTAGTCGTTAC		
NB11_100/101/103A_fwd	Sigma-Aldrich	N/A
CCAAAGCCAGTTCGTAACGACTA GCACCTGCGGCCTTCGCCGCACA GTAATACACGG		

(*Continued on next page*)

Continued

REAGENT or RESOURCE	SOURCE	IDENTIFIER
NB11_100/101/103A_rev	Sigma-Aldrich	N/A
CCGTGTATTACTGTGCGGCGAAG GCCGCAGGTGCTAGTCGTTACGA ACTGGCTTTGG		
NB11_L103A_fwd	Sigma-Aldrich	N/A
CCAGTTCGTAACGACTAGCACC TAAGAGCTTCGCCG		
NB11_L103A_rev	Sigma-Aldrich	N/A
CGGCGAAGCTCTTAGGTGCTAGTCGT TACGAACTGG		
pHen6c_G5_His	Sigma-Aldrich	N/A
AGGTCACCGTCTCCTCAG		
GGGGTGGAGGCGGCCTGCCGAG CACCGGTGGCCATCATCACCATC ACCACTAATAGAATTCACTGGCCGTC		
pHen6c_G5_Ct_fwd	Sigma-Aldrich	N/A
TAGAATTCACTGGCCGTCGTTTTACAAC		
pHen6c-G5-Ct-rev	Sigma-Aldrich	N/A
TGAGGAGACGGTGACCTGGGT		
Nb_pHen6C_Srt_fwd	Sigma-Aldrich	N/A
CAGGTGCAGCTGCAGGAGTC		
Nb_pHen6C_Srt_rev	Sigma-Aldrich	N/A
TGAGGAGACGGTGACCTGGGTCC		
pHen6C_Srt_F1	Sigma-Aldrich	N/A
CCCAGGTCACCGTCTCCTCA		
pHen6C_Srt_R1	Sigma-Aldrich	N/A
GACTCCTGCAGCTGCACCTG		
Recombinant DNA		
pHen6C with Nb9 insert	This Study	N/A
pHen6C with Nb11 insert	This Study	N/A
Phen6c with Nb14 insert	This Study	N/A
Phen6c with Nb19 insert	This Study	N/A
Phen6c with sortaggable Nb9 insert	This Study	N/A
Phen6c with sortaggable Nb11 insert	This Study	N/A
pcDNA3.1 with sortaggable heavy chain Nb11	This Study	N/A
Phen6c with sortaggable Nb14 insert	This Study	N/A
Phen6c with sortaggable Nb19 insert	This Study	N/A
Phen6c with Nb11 100A mutant	This Study	N/A
Phen6c with Nb11 103A mutant	This Study	N/A
Phen6c with Nb11 100/101/103A mutant	This Study	N/A
Phen6c with Nb19 114A mutant	This Study	N/A
Phen6c with Nb19 115A mutant	This Study	N/A
Phen6c with Nb11 114/115A mutant	This Study	N/A
Phen6c with 'irrelevant NB' BabA	This Study	N/A
Software and algorithms		
COOT	Emsley et al., 2010	https://www2.mrc-lmb.cam.ac.uk/personal/pemsley/coot/
Phenix Software Suit	Adams et al., 2010	https://phenix-online.org/
Chimera	Pettersen et al., 2004	https://www.cgl.ucsf.edu/chimera/

(*Continued on next page*)

Continued

REAGENT or RESOURCE	SOURCE	IDENTIFIER
CCP4 Software Suit	Collaborative Computational Project, Number 4, 1994	http://legacy.ccp4.ac.uk
iMosfilm	Battye et al., 2011	https://www.mrc-lmb.cam.ac.uk/harry/imosflm
AutoProc	Vonrhein et al., 2011	http://www.globalphasing.com/autoproc/
XIA2/DIALS	Winter et al., 2013	https://dials.github.io/index.html
Imaris x64 Version 9.5.1	Oxford Instruments	https://imaris.oxinst.com/
Prism Version 8.4.3 and Version 9.1.2	GraphPad	https://www.graphpad.com
Fiji (ImageJ v2.0.0)	Rueden et al., 2017	https://fiji.sc
CellQuest Pro 6.0	Becton Dickinson Bioscience	N/A
Live Acquisition Software	Thermo Fisher Scientific	N/A
Offline Analysis	Thermo Fisher Scientific	N/A
Other		
HiLoad 16/600 Superdex	GE Healthcare	N/A
24 well plate	Sarstedt	83.3922.500
PD10 columns	Thermo Fisher	29922
Slide-A-Lyzer	Thermo Fisher	P00090074
Cell culture flasks	Merck	C7481-50EA
Vivaspin 500	Sartorius	VS0191
Amicon stirred cell	Merck	UFSCO5001
Amicon filtration membrane	Merck	PCGC04310
24 Well Hanging Drop Vapor Diffusion Plate	Jena Bioscience	CPL-132

RESOURCE AVAILABILITY

Lead contact

Further information and requests for resources and reagents should be directed to and will be fulfilled by the Lead Contact, Erec Stebbins.

Materials availability

Plasmids generated from this study can be obtained directly from the Lead Contact.

Data and code availability

The following structure files are available from the Protein Databank: PDB: 7AQX, 7AQY, 7AQZ, and 7AR0. This paper does not report original code. Any additional information required to reanalyze the data reported in this paper is available from the lead contact upon request.

EXPERIMENTAL MODEL AND SUBJECT DETAILS

The following Eukaryotic cell lines were used: FreeStyle 293 F cells, *Trypanosoma brucei brucei* 2T1 and *Trypanosoma brucei brucei* Lister 427, clone 221. The Freestyle 293 F cells were obtained from Thermo Fisher (Resource table). The *Trypanosoma brucei brucei* 2T1 were originally created in the laboratory of David Horn, University of Dundee, and *Trypanosoma brucei brucei* Lister 427, clone 221 were obtained from George Cross, Rockefeller University.

Trypanosoma brucei brucei 2T1 and Lister 427, clone 221 were grown in a humidified 37°C incubator with 5% CO_2 using HMI-9 medium (PAN Biotech) supplemented with 10% FBS (GIBCO), 1.5 mM L-cysteine (SERVA) and 0.2 mM β-mercaptoethanol (SIGMA). Cells were maintained below 5×10^5 cells/mL and only grown to a density of 4×10^6 cells/mL prior to harvesting. Freestyle 293 F cells were maintained in FreeStyle 293 Expression Medium (Thermo Fisher, 12338018). Cell were maintained below 1×10^6 cells and only allowed to grow to higher density after transfection.

METHOD DETAILS

Production of nanobodies

Nanobodies (Nbs) were produced by the VIB Nanobody Core (Vrije Universiteit Brussel). A llama was subcutaneously injected on days 0, 7, 14, 21, 28 and 35, each time with 150 μg of the N-terminal domain of VSG2 from *Trypanosoma brucei brucei*. The adjuvant used was Gerbu adjuvant P. On day 40, about 100 mL of anticoagulated blood was collected from the llama for lymphocyte preparation. A VHH library was constructed from the llama lymphocytes to screen for the presence of antigen-specific nanobodies. To this end, total RNA from peripheral blood lymphocytes was used as template for first strand cDNA synthesis with an oligo(dT) primer. Using this cDNA, the VHH encoding sequences were amplified by PCR, digested with PstI and NotI, and cloned into the PstI and NotI sites of the phagemid vector pMECS. The library consists of about 7×10^8 independent transformants, with 100% of transformants harboring the vector with the right insert size (size of the DNA sequences coding for VHHs). The library was panned for 3 rounds in solution on inactivated, UV-irradiated *Trypanosoma brucei brucei* cells expressing VSG2. Phages from the library were incubated with the *Trypanosoma brucei brucei* cells after which the cells were washed and the binding phages were eluted. The enrichment for antigen-specific phages was assessed after each round of panning by comparing the number of phagemid particles eluted from *Trypanosoma brucei brucei* cells (output) with the number of phagemid particles used for panning (input). The phage outputs for the 1st, 2nd and 3rd rounds were about 5×10^4, 5×10^4 and 1.5×10^7, respectively. The phage output increased about 30-fold in the 3rd round, as compared to the outputs from the 1st and 2nd rounds. The input phage was consistently near 10^{11}. In total, 190 colonies (95 from round 2 and 95 from round 3) were randomly selected for sequencing. After removal of redundant sequences, there were 89 unique VHH sequences belonging to 46 different CDR3 groups (B cell lineages). The crude periplasmic extracts from representatives of all CDR3 groups were tested by flow cytometry for their specificity for the target antigen, using inactivated fixed *Trypanosoma brucei brucei* cells. An irrelevant nanobody (a nanobody specific for *Helicobacter pylori* BabA antigen) served as negative control. A mouse anti-VSG2 mAb was used as positive control. Based on flow cytometry data and B cell lineage data, 69 different positive nanobodies were identified, belonging to 30 different CDR3 groups (B cell lineages). The nanobodies were sub-cloned into pHEN6c vector and expressed in WK6 cells.

The PCR reaction was performed using Q5 High-Fidelity DNA Polymerase PCR kit (10 μL Q5 Reaction Buffer 5x, 1 μL 10 mM dNTPs, 2.5 μL Primers, 10 ng template DNA, 0.5 μL Q5 polymerase, 10 μL 5X Q5 High GC Enhancer and filled up to 50 μL with H_2O). Amplification of the Nb insert by PCR was using pMECS plasmids harboring the nanobody gene as template and the reaction contained 30 cycles of PCR, each cycle consisting of 30 s at 94°C, 30 s at 55°C and 45 s at 72°C, followed by 10 minutes extension at 72°C at the end of PCR. A fragment of about 400 bp was amplified and can be visualized on a 1% agarose gel. The amplified insert was introduced to a pHEN6c backbone using standard ligation techniques following the Roche dephosphorylation and ligation kit instructions.

Expression was induced by overnight growth in TB medium at 28°C with 1 mM IPTG addition at an OD600 of 0.6-0.8 (final OD600 after overnight induction was typically between 25 and 30). Cells were lysed by osmotic shock in TES buffer (0.2 M Tris pH 8.0, 0.5 mM EDTA, 0.5 sucrose) and the clarified supernatant incubated with Ni-NTA slurry (QIAGEN, Germany). After washing with PBS, the protein was eluted with 0.5 M imidazole and then dialyzed against PBS.

Production of nanobody mutants

Nanobody mutants (NB11 L101A and NB19 E114A, Y115A, and E114/Y115A) were produced using the Q5 High-Fidelity DNA Polymerase PCR kit (10 μL 5x Q5 Reaction Buffer, 1 μL 10 mM dNTPs, 2.5 μL Primers, 10 ng template DNA, 0.5 μL Q5 Polymerase, 10 μL 5X Q5 High GC Enhancer filled up to 50 μL with H_2O) with primers designed to create the desired mutations. PCR settings were 98°C for initial denaturation (30 s) followed by 35 cycles of 98°C (10 s), 72°C (30 s) and 72°C (2 min). Final extension was 72°C for 2 min. The PCR product was gel purified and 50 ng of the product was used in the NEBuilder HiFi DNA Assembly kit. After incubation for 1 h at 60°C 2.5 μL were used in standard transformation experiments. Nanobody mutants for NB11 L100A, L103A, and L100/L101/S103A were produced using the instructions of the QuickChange Lightning kit (Agilent) at a PCR reaction temperature of 68°C. Successful reactions were used for standard transformation experiments. All clones were verified by DNA sequencing. Expression and purification of positive clones was performed as described before for wild-type nanobodies. Complex formation was performed as described before for the wild-type, but with less protein (1 mg each corresponding to a 1:4 molar ratio).

Production of sortaggable nanobodies

Sortaggable Nbs were created by cloning a DNA fragment encoding *Streptococcus pyogenes* Sortase A recognition peptide (LPSTGG) flanked by a flexible penta-glycine linker and hexa-histidine tag to the Nb-CTD sequence. A pHen6c vector was modified to harbor a penta-glycine and hexa-histidine tag using Q5 High-Fidelity Polymerase (NEB) and HiFi Assembly Mix as described above. Next, Nb sequences were subcloned into this new vector, using the Q5 High-Fidelity Polymerase (NEB) and HiFi Assembly Mix (NEB) as described above. Successful reactions were sent for sequencing and positive plasmids used in standard transformation experiments.

Synthesis of a His-tagged VSG2-irrelevant nanobody (NB-ER19)

A nanobody generated against *Helicobacter pylori* adhesin BabA has been described before (Moonens et al., 2016, ''NB-ER19'') and was used as a negative control in biopanning of the M13 phage display VHH library on UV-irradiated *Trypanosoma brucei* cells expressing VSG2 by VIB. A codon-optimized DNA encoding NB-ER19 was synthesized and cloned into pHen6C plasmid (primers in Key Resource table) using Q5 High-Fidelity DNA polymerase (NEB) as previously described.

The pHEN6C-ER19 plasmid encoding ER19 nanobody with a C-terminal His-tag was transformed into *E. coli* WK6 competent cells and purified after IPTG induction as described before.

Purification of VSG2

Trypanosoma brucei brucei expressing VSG2 were cultivated *in vitro* in HMI-9 media (formulated as described by Hirumi and Hirumi, 1991 by PAN Biotech without FBS, L-cysteine, or β-mercaptoethanol), supplemented with 10% fetal calf serum (GIBCO), 1.5 mM L-cysteine, and 0.2 mM β-mercaptoethanol. Cells were cultured at 37°C with 5% CO_2. VSG2 was purified according to established protocols (adapted from Cross, 1984). Briefly, cells were pelleted (20 min, 3200 *xg*, 4°C) and then lysed in 0.2 mM ice-cold $ZnCl_2$. The lysis mixture was centrifuged for 10 min at 10000 *xg* at 4°C (SN0) and the pellet containing the membrane material was resuspended in pre-warmed (42°C) 20 mM HEPES buffer, pH 8.0 with 150 mM NaCl. Following a second centrifugation, supernatant containing VSG protein (SN1 + SN2) was loaded onto an anion-exchange column (Q-Sepharose Fast-Flow, GE Healthcare), which had been equilibrated with 20 mM HEPES buffer, pH 8.0 with 150 mM NaCl. The flow-through containing highly pure VSG was concentrated in an Amicon Stirred Cell and optionally shock frozen in liquid nitrogen and stored at −80°C. For crystallization experiments the C terminus of VSG2 was cut using 1 μg Endoproteinase LysC per 1 mg of VSG2. Digest was performed for 90 min at room temperature. A final step of purification involved gel filtration on a HiLoad 16/600 Superdex 200pg column (GE Healthcare) in 20 mM HEPES pH 8.0, 150 mM NaCl.

Purification and crystallization of VSG2-nanobody complexes

Purified NTD VSG2 (in 20 mM HEPES pH8.0, 150 mM NaCl) and purified nanobody (in PBS) were mixed in a ratio of 1:4, resulting in a final buffer of 5 mM HEPES pH 8.0, 139.5 mM NaCl, 2 mM KCl, 6 mM Na_2HPO_4, and 1.5 mM KH_2PO_4. The VSG2-nanobody complex was further purified by gel filtration on a HiLoad 16/600 Superdex 200pg column in 10 mM Tris pH 8.0. VSG2-nanobody complexes were concentrated to 5-8 mg/mL. Crystals were grown by vapor diffusion using hanging drops formed from mixing a 1:1 volume ratio of the protein with an equilibration buffer consisting of 20% PEG 1500, 0.1 M citrate (VSG2-NB9), 0.1 M imidazole, 19% PEG 1500 (VSG2-NB11), 0.1 M citrate, 23% PEG 1500 (VSG2-NB14) and 0.1 M ADA pH 6.5, 2 M ammonium sulfate, and 0.1 M magnesium sulfate (VSG2-NB19). Samples were cryo-protected by transfer of the crystals into a buffer of the crystallization solution augmented with 10%–20% PEG 400.

Structure determination of VSG2-nanobody complexes

VSG2-nanobody datasets were collected at the Paul Scherrer Institut Villingen, (SLS) and Diamond Light Source. All structures were solved by molecular replacement with the PHENIX software suite ((Adams et al., 2010), specifically, PHASER (McCoy et al., 2007)) using the PDB entries 1VSG and ChainB of 5lhr as the search models. Refinement with PHENIX coupled to cycles of manual rebuilding produced the final models of the complexes (Table S2).

Cloning, expression, purification, and sortagging of camelid VHH-IgG2 heavy chain antibodies

A DNA fragment containing the hinge region from camel IgG2, CH2, CH3, *Streptococcus pyogenes* Sortase A acceptor sequence (LPSTGG) and a His-tag was codon-optimized for *Homo sapiens* codon usage and synthesized as a clone in pcDNA3.1 plasmid. Next, the VHH domains were PCR amplified from pHen6c plasmids using Q5 DNA polymerase (NEB) as previously described using the primer NB-Cam-IgG2-fwd and NB-Cam-IgG2-rev (Key Resource Table). pcDNA3.1 plasmids containing Camelid heavy chain IgG2 were linearized by PCR using the primer cHc-Cam-IgG2-fwd and cHc-Cam-IgG2-rev (Key Resource Table) as described before. Finally, the pcDNA3.1-IgG2 vector and the VHH amplicons were assembled to create pcDNA3.1-VHH-IgG2 expression plasmids, using HiFi DNA Assembly Master Mix as described before.

The pcDNA3.1 plasmid containing VHH-IgG2 heavy-chain antibody was transiently transfected into suspension cultures of FreeStyle 293-F cells in FreeStyle 293 Expression Medium using 293fectin Transfection Reagent as recommended by the manufacturer (Life Technologies). Culture supernatants were collected and filter sterilized. Purification was done using Ni-NTA agarose resin (QIAGEN). The equilibrated resin was incubated with the supernatant and left gently shaking for 1 h at 4°C. Afterward the column was washed with 5 column volumes of 20 mM Tris pH 8.0, 30 mM imidazole and 0.3 M NaCl. Finally, the antibodies were eluted with 250 mM imidazole, 20 mM Tris pH 8.0, 30 mM imidazole and 0.3 M NaCl, followed by removal of imidazole by Slide-A-Lyzer dialysis cassette (10 kDa MWCO, Life Technologies) and concentration by Amicon-15 ultrafiltration unit (10 kDa MWCO, Millipore). Sortagging reactions were done using 2 mg of antibodies, 100 μM *Streptococcus pyogenes* Sortase A and 500 μM AAGG-5-FAM peptide (Biomatik, USA) in PBS overnight at 4°C. Excess AAGG-5-FAM FAM-peptide was removed by a gel filtration column (GE Healthcare) as recommended by the manufacturer. Finally, Sortagged heavy chain IgG2 antibodies were concentrated using an Amicon 15 ultrafiltration unit (3 kDa MWCO, Millipore) and the concentrations were measured using BCA assay kit (Life Technologies) using a BSA standard curve.

Sortagging of VSG2 nanobodies

Sortaggable versions of VSG2 nanobodies, expressed by pHen6C-Srt plasmids, were purified from WK6 cultures after IPTG induction, using a Ni-NTA agarose resin (QIAGEN, Germany), similar to non-sortagged nanobodies. A peptide (AAGG-5-FAM) carrying a C-terminal 5-FAM was synthesized and purified by HPLC (Biomatik, USA). His-tagged Sortase A derived from *Streptococcus pyogenes* was produced in BL21-DE3 using pSpSortA-pET28a plasmid and purified as previously described (Pinger et al., 2017). Sortagging reactions were performed using 1 mg of nanobody, 75 μM Sortase A and 350 μM FAM-labeled peptide in PBS overnight at 4°C. Excess FAM-peptide was removed by a gel filtration column (GE Healthcare). Finally, Sortagged nanobodies were concentrated using an Amicon 15 ultrafiltration unit (3 kDa MWCO, Millipore) and the concentrations were measured using BCA assay kit (Life Technologies) using a BSA standard curve.

Flow cytometry analysis of heavy chain IgG2 binding to the native VSG2 coat on *T. brucei*

2×10^6 2T1 cells expressing VSG2 were centrifuged at 6000 x*g* for 10 min at 4°C and resuspended in 200 μL cold HMI-9 media and incubated with a 4-fold molar excess FAM-sortagged reconstructed Camelid IgG2(NB11) antibody (relative to VSG2) and left at 4°C for 10 min with gentle shaking. The unbound antibodies were washed away with a cycle of adding the volume to 2 mL and afterward centrifuging at 6000 x*g* for 10 min at 4°C. The washed cell pellet was resuspended in 200 μL cold HMI-9 medium for flow cytometry analysis (FACSCalibur, BD). Non-stained 2T1 cells were used as a control.

Flow cytometry analysis of nanobodies binding to the native VSG2 coat on *T. brucei*

2×10^6 2T1 cells expressing VSG2 were centrifuged at 6000 x*g* for 10 min and resuspended in 200 μL cold HMI-9 medium. The resuspended pellet was stained with 4-fold molar excess of $NB9_{VSG2}$, $NB11_{VSG2}$, $NB14_{VSG2}$, and $NB19_{VSG2}$, relative to VSG2, and left at 4°C for 10 min with gentle shaking. The excess unbound nanobodies were washed away with a cycle of resuspending in 2 mL cold HMI-9 medium followed by centrifuging at 6000 x*g* for 10 min at 4°C. The washed pellet was resuspended in 200 μL HMI-9 medium and incubated with anti-His antibody (1:1000) in cold HMI-9 medium at 4°C for 10 min with gentle shaking. Samples were resuspended in 2 mL cold HMI-9 medium as an additional wash step and centrifuged at 6000 x*g*. Samples were resuspended in 200 μL cold HMI-9 medium prior to flow cytometry analysis. Controls were established by using non-treated parasites (2T1) and parasites (2T1) treated with anti-His antibody.

Flow cytometry analysis of FAM-sortagged nanobodies binding to the native VSG2 coat on *T. brucei*

Sortaggable versions of VSG2 nanobodies were purified as mentioned above. 2×10^6 2T1 cells expressing VSG2 were centrifuged at 6000 x*g* for 10 min and resuspended in 200 μL cold HMI-9 medium. The resuspended pellet was stained with 4-fold molar excess FAM-sortagged nanobodies at 4°C for 10 min with gentle shaking. The excess nanobodies were washed away with a cycle of resuspending in 2 mL cold HMI-9 medium followed by centrifuging for 10 min at 6000 x*g*. The washed pellet was resuspended in 200 μL cold HMI-9 medium for flow cytometry analysis (FACSCalibur, BD). Non-stained 2T1 cells were used as a control.

Flow cytometry analysis of $NB11_{VSG2}$ binding to different native VSG coats on *T. brucei*

2×10^6 2T1 cells expressing either VSG531, VSG615 or VSG1954 were centrifuged at 6000 x*g* for 10 min at 4°C and resuspended in 200 μL cold HMI-9 medium. The resuspended pellets were stained with 4-fold molar excess of $NB11_{VSG2}$ relatively to VSG2 at 4°C for 10 min with gentle shaking. The excess nanobodies were washed away with a cycle of resuspending in 2 mL cold HMI-9 medium followed by centrifuging at 6000 x*g* for 10 min. The washed pellets were resuspended in 200 μL cold HMI-9 medium and incubated with anti-His antibody (1:1000) in cold HMI-9 medium at 4°C for 10 min with gentle shaking. Samples were washed by a cycle of resuspending in 2 mL cold HMI-9 medium and centrifuging at 6000 x*g* for 10 min. Samples were resuspended in 200 μL HMI-9 medium for flow cytometry analysis (FACSCalibur, BD). Non-stained 2T1 cells and 2T1 cells only incubated with anti-His antibody were used as a control.

Flow cytometry analysis of FITC-conjugated nanobodies binding to the native VSG2 coat on *T. brucei*

Nbs were conjugated using the FITC Conjugation Kit – Lightning Link from abcam (ab102844). 20 μg Nbs were mixed with 2 μL of the modifier reagent and afterward incubated with 10 μg of the fluorescent material. Samples were left at room temperature for 3 h and the reaction was stopped using 2 μL of the quencher reagent. 2×10^6 2T1 cells expressing VSG2 were centrifuged at 6000 x*g* for 10 min at 4°C and stained with 4-fold molar excess FITC-conjugates (relative to VSG2) in cold HMI-9 medium at 4°C for 10 min with gentle shaking. The excess nanobodies were washed away by resuspending in 2 mL cold HMI-9 medium and centrifuging for 10 min at 6000 x*g* at 4°C afterward. The cells were resuspended in 200 μL HMI-9 medium for flow cytometry analysis (FACSCalibur, BD). Non-stained 2T1 cells were used as a control.

Western blot analysis

2×10^6 2T1 cells expressing VSG2 were centrifuged at 6000 x*g* for 10 min and resuspended in 200 μL cold HMI-9 medium. The resuspended pellet was stained with 4-fold molar excess of $NB9_{VSG2}$, $NB11_{VSG2}$, $NB14_{VSG2}$, $NB19_{VSG2}$ and NB-ER19 (BabA), respectively, and left at 4°C for 10 min with gentle shaking. The excess nanobodies were washed away with three cycles of resuspending in 2 mL cold HMI-9 medium and centrifuging at 6000 x*g* for 10 min at 4°C afterward. The washed pellet was resuspended in 200 μL cold HMI-9 medium and Laemmli-Buffer was added to a final concentration of 1x.

Samples were run on SDS-PAGE (4%–15%) at 120 V for 50 minutes. Proteins were transferred to a Nitrocellulose membrane by applying 100 V for 75 minutes in the cold using standard western blot protocols. Transferred membrane was blocked by incubating in 10 mL 3% milk in TBS-T at 4°C for 1 h. After washing, the membrane was incubated with primary antibody (anti-His (rabbit) 1:1000 and anti-α-Tubulin 1:3000 (rabbit)) in blocking solution overnight at 4°C. Excess primary antibody was washed away with three cycles of washing with TBS-T. Secondary antibody (rabbit, 1:2000 for anti-His antibody, 1:5000 for anti-α-Tubulin antibody) was applied by incubating in blocking solution for 1 h at 4°C. Membrane was then washed 3 times with TBS-T. Membrane was treated with ECL substrate and bands were visualized using the GelDoc system.

T. brucei culturing for motility and toxicity assays

All motility and subsequent toxicity, electron microscopy and immunofluorescence assays were performed on VSG2 expressing wild-type cells (Lister 427, clone 221) as preliminary experiments (not shown) found these to be more robust swimmers compared to other VSG2 expressing cell lines such as 2T1 or 13.90 cells. VSG6 expressing wild-type cells (Lister 427, clone 121) were used in control experiments to show specificity. Trypanosomes were cultivated at 37°C and 5% CO_2 in HMI-9 cell culture medium containing 10% heat-inactivated fetal calf serum and generally maintained below a density of 5×10^5 cells/mL.

Cell viability assay via flow cytometry

For each preparation of cells for flow cytometry analysis, 1.4×10^7 cells were harvested by centrifugation at 1500 x*g* for 10 min at room temperature. The cell pellet was washed with 4 mL of pre-warmed and filtered (pore size 0.22 μm) HMI-9 and centrifuged at 1500 x*g* for 5 min at room temperature. All but 1 mL of the supernatant was discarded to achieve a cell density of 1.4×10^7 cells/mL. The cell suspension was transferred to a 24-well plate for incubation at 37°C and 5% CO_2 for the duration of the time course. Alongside a no nanobody control the required amount of nanobody (ranging from a 0.3- to 10-fold molar excess of nanobody to VSG2 monomer present on the cells) was added per well and subsequent gentle agitation of the plate ensured mixing with the cell suspension. At various time points during incubation, 50 μL of the cell suspension were removed and diluted with 250 μL of filtered HMI-9. Cells were then incubated for 10 min with 1 μg of propidium iodide (PI) which serves as a dead cell fluorescence marker. The ratio of fluorescent, dead cells to non-fluorescent living cells was analyzed with a FACSCalibur Flow Cytometer and the CellQuest Pro software (Becton Dickinson Bioscience, Franklin Lakes, USA).

Tracking of individual cells in a population

For analysis of cell trajectories, 1.4×10^6 cells were harvested by centrifugation at 1500 x*g* for 10 min at room temperature and re-suspended in 50 μL HMI-9 medium. An equal volume of MC-HMI-9 medium (HMI-9 medium containing 1.1% methylcellulose (MO512, Sigma Aldrich, St. Louis, USA)) was added to reach a viscosity of 25 mPa·s and a cell density of 1.4×10^7 cells/mL. The respective nanobodies were added to a final concentration of 6 μg/mL, resulting in an approx. 1.7-fold molar excess of nanobody to VSG2 monomer present on the cells. For data acquisition 3 μL of the cell suspension was placed on a slide and covered with a coverslip. In a pilot experiment recordings of 30 min duration starting 5 min post addition of the nanobody were acquired with a stereomicroscope (Leica MZ16FA, Leica Microsystems, Mannheim, Germany) equipped with a Plan Apo 5x LWD objective (Leica Camera AG, Wetzlar, Germany), a zoom factor of 35x, and a CCD pco.1600 camera (PCO, Kelheim, Germany) employing an exposure time of 250 ms. In subsequent experiments videos of 125 s were acquired at 5, 15, 25 and 35 min post addition of the respective nanobody and the field of view was changed in between recordings to ensure adequate cell numbers for analysis. Trajectories were visualized and analyzed with the Imaris x64 software (Version 9.5.1, Oxford Instruments).

High-speed microscopy of single cells

High-speed microscopy was performed to analyze effects on motility on a single cell level. Cells were prepared as for ensemble measurements described above but using a final cell density of 7×10^6 cells/mL. High-speed videos were captured with an inverted fully automated DMI 6000B wide-field microscope (Leica Microsystems, Mannheim, Germany) equipped with a Leica 63x glycerol immersion objective (NA 1.3) (Leica Microsystems, Mannheim, Germany) and an sCMOS camera (PCO, Kelheim, Germany) using a frame rate of 250 fps.

Fluorescence recovery after photobleaching (FRAP) experiments

A total of 1×10^7 cells were harvested and washed three times with ice-cold TDB (5 mM KCl, 80 mM NaCl, 1 mM $MgSO_4$, 20 mM glucose, 20 mM Na_2HPO_4, 2 mM NaH_2PO_4, pH 7.6) and centrifuged at 1500 x*g* and 4°C for 10 min. Following this, TDB was added to achieve a final cell density of 1×10^8 cells/mL and trypanosomes were incubated with a final concentration of 10 μM ATTO 488 NHS-ester for 15 min on ice in the dark to label the cell surface. Cells were washed three times with 1 mL ice-cold TDB to remove all unbound dye. Following the final wash, the labeled cells were resuspended in 20 μL TDB and $NB11_{VSG2}$ was added to a 1.7-fold molar excess over VSG2 monomer present (4.3 μg). For immobilization, 3 μL of cell suspension were mixed with 5 μL of 10% (w/v) type A gelatin (from porcine skin; Sigma-Aldrich) in PBS, pH 7.8, which was pre-warmed to 37°C, and placed between two cleaned and also pre-warmed coverslips. These were then mounted in a temperature-controlled sample holder that was cooled to 21°C for data acquisition. Coverslips were cleaned by two 10 min sonication steps (37 kHz, 320 W, sweep mode) in 2% Hellmanex followed by at least one further sonication step in ultrapure water. Coverslips were rinsed thoroughly in ultrapure water following each sonication step.

To avoid analysis of dead cells, data acquisition was restricted to 60 minutes following nanobody addition and care was taken to analyze only those cells that showed residual beating of the free flagellar tip in the otherwise immobilized cells.

To determine the diffusion coefficient and mobile fraction of VSG on living trypanosomes, line fluorescence recovery after photobleaching (line-FRAP) experiments were performed. For this, an inverted, fully automated wide-field microscope (FEI Munich GmbH, Germany), equipped with a Polychrome V monochromator (FEI Munich GmbH, Germany), a Yanus digital scan head (FEI Munich GmbH, Germany) for the control of 473 nm and 561 nm lasers (Cobolt Inc, Solna, Sweden), appropriate excitation and emission filters, a CCD camera (Sensicam, 6.45 μm/px; PCO, Kelheim, Germany) and a 60x oil immersion objective (NA 1.45) (Nikon, Tokyo, Japan) were used. Live Acquisition software (FEI Munich GmbH, Germany) was used for data acquisition. In every experiment, 10 pre-bleaching images (I_{pre}) were acquired with 100 ms exposure time in a cycle of 500 ms. A line-shaped area ($I_{FRAP}(t)$) was then irreversibly bleached with a 20 ms laser pulse at 25% laser intensity. To monitor the fluorescence recovery in ($I_{FRAP}(t)$), 150 images were acquired after bleaching with 100 ms exposure time at intervals of 500 ms.

Data were analyzed using the Offline Analysis software packages (FEI Munich GmbH, Germany) according to Phair et al. and Hartel et al. (Phair et al., 2004, Hartel et al., 2015).

Sample preparation for SEM

To prepare samples for SEM, 1.4×10^7 cells were harvested by centrifugation at 1500 x*g* for 10 min at room temperature and resuspended in 750 μL HMI-9 medium. Cells were then generally treated with a 1.7-fold molar excess of the different nanobodies (6 μg) for the desired durations of time. One experiment was conducted using a 0.85:1 molar ratio of $NB11_{VSG2}$ to VSG monomer present. VSG2 expressing cells that were prepared and incubated as above with the omission of Nb addition and NB11VSG2 treated VSG6 expressing cells served as negative controls. After incubation, 250 μL of 25% glutaraldehyde were added and cells were fixed for 1 h at room temperature. The fixative was removed by washing once with Sørensen buffer (18.2% of 60 mM KH_2PO_4, 81.8% of 60 mM Na_2HPO_4, pH 7.4) with centrifugation at 1500 x*g* for 5 min at 4°C. Following resuspension of the cells in fresh buffer they were spun onto polylysine coated coverslips at 1500 x*g* and 4°C for 10 min and washed twice with Sørensen buffer. Coverslips with attached trypanosomes were transferred into critical point drying vessels and dehydrated at 4°C for 5 min each in a series of 30%, 50%, 70%, 90%, 100% (5x) acetone. This was followed by an overnight incubation in 100% acetone and subsequent critical point drying (CPD) according to the manufacturer's instructions (Mulisch and Welsch, 2015). Coverslips were then attached to specialized racks and connected by a thin layer of conductive silver. Finally, samples were vapor plated with gold-palladium for 150 s. A JSM-7500F Scanning Electron Microscope (JEOL, Tokyo, Japan) was used for imaging.

Chemical fixation and subsequent Epon embedding for TEM

During chemical fixation, 6×10^7 cells were harvested by centrifugation at 1500 x*g* for 10 min at room temperature and all except 900 μL of supernatant was removed. Nanobody was added to an approximate 1.7-fold molar excess compared to VSG2 monomer present (24 μg) and incubated for the desired time. Negative controls were prepared in the same way except for omission of Nb addition. Following incubation, cells were fixed by adding 100 μL of 25% glutaraldehyde and incubating for 1 h at room temperature. The samples were then washed 5 times with 1 mL 0.05 M cacodylate-buffer (pH 7.2). For this, samples were centrifuged at 1500 x*g* for 5 min, the supernatant was removed, and fresh buffer added while taking care not to resuspend the cell pellet. For a second fixation and for contrasting, cell pellets were incubated with 100 μL 2% OsO_4 in 0.05 M cacodylate-buffer for 1 h at 4°C. Samples were washed 5 times with pure H_2O for 3 min each (centrifugation was omitted unless the pellet became dislodged). Subsequently, 1 mL 0.5% uranyl acetate was added before overnight incubation at 4°C. Cells were again washed 5 times with pure H_2O for 3 min each. To dehydrate the samples, the pellets were incubated sequentially for 30 min each at 4°C with 50%, 70%, 90%, and finally 100% EtOH. This was followed by two 30 min incubations with 100% EtOH, and three 30 min incubations with propylene oxide at room temperature. Then, 50% Epon in propylene oxide was added and incubated overnight as the first embedding step, followed by two incubation steps with 100% Epon for 2 h each. Finally, Epon was exchanged one last time and polymerized at 60°C for at least 48 h.

High-pressure freezing and Epon embedding for TEM

Generally, 2.8×10^7 cells were harvested by centrifugation at 750 x*g* for 3 min at room temperature. The supernatant was reduced to a residual amount of 1 mL medium and 1 mL heat-inactivated fetal calf serum was added as a cryoprotectant. Nanobody was added to a 1.7-fold excess compared to VSG2 monomer present (12 μg total) and incubated for various durations of time. As a negative control, cells were prepared and incubated as described above but without the addition of nanobody. Following incubation, samples were centrifuged at 750 x*g* for 3 min at room temperature. All but around 200 μL of supernatant was removed and the cell pellet was resuspended carefully. The cell suspension was transferred into a PCR tube and centrifuged for 10 s at room temperature and 2000 x*g* with subsequent removal of most of the supernatant. Cells were then transferred to the freezing chamber (specimen carrier type A (100 μm) and specimen carrier type B (0 μm)). High-pressure freezing was performed with an EM HPM100 (Leica Microsystems, Mannheim, Germany) at a freezing speed of > 20000 Ks^{-1} and a pressure of > 2100 bar. Samples were stored in liquid nitrogen until embedding.

For Epon embedding, the frozen samples were transferred into an EM AFS2 automated freeze substitution system (Leica Microsystems, Mannheim, Germany) and incubated in 0.5% (v/v) glutaraldehyde and 0.1% (w/v) tannic acid in anhydrous acetone for 96 h at −90°C. The solution was changed once after 24 h. After incubation, the samples were washed four times with anhydrous acetone

at −90°C for 1 h each and finally contrasted in 2% (w/v) OsO_4 in anhydrous acetone for 28 h at −90°C. Following this, the temperature was raised to −20°C within 14 h, left at −20°C for 16 h, and increased to 4°C within 4 h. Then the samples were washed four times with anhydrous acetone at 4°C over a period of 2-3 h. Finally the temperature was adjusted to 20°C over a time of 1 h. Cell pellets were removed from the carriers and transferred into 50% Epon in acetone. After 5 h the Epon was exchanged with 90% Epon in acetone, and left overnight at 4°C. The next day, samples were incubated three times with 100% Epon for 2 h each at room temperature. Polymerization occurred at 60°C for a minimum of 24 h.

Preparation of stained and contrasted sections for TEM analysis

An Ultra Jumbo Diamond Knife (Diatome AG, Nidau, Switzerland) was used to cut 60 nm serial sections of Epon embedded samples. Sections were placed on pioloform coated slotted copper grids and incubated for 10 min with 2% uranyl acetate in ultrapure H_2O, followed by incubation for 5 min with Reynolds' lead citrate. Images were acquired with a 200 kV JEM-2100 (JEOL, Tokyo, Japan) transmission electron microscope equipped with a TemCam F416 4k x 4k camera (Tietz Video and Imaging Processing Systems, Gauting, Germany).

Immunofluorescence assays

For immunofluorescence imaging, 3×10^6 cells were harvested by centrifugation at 750 x*g* for 5 min at room temperature. The cells were washed by resuspending in 5 mL of serum-free HMI-9 and again centrifuging at 750 x*g* for 5 min at room temperature. Then, the cell pellet was resuspended in 200 μL serum-free HMI-9 to achieve a cell density of 1.4×10^7 cells/mL. Nanobody was added in a 1.7-fold molar excess compared to VSG2 present in the sample followed by incubation for 15 min at room temperature. After incubation, the samples were brought to a final volume of 1 mL with serum-free HMI-9 and fixed for 30 min at room temperature with a final concentration of 4% formaldehyde. Fixed cells were washed with TDB and pelleted by centrifugation at 750 x*g* for 5 min following which most of the supernatant was removed. Cells were resuspended in the residual supernatant and applied to polylysine coated slides and left to settle for 1 h. Slides were washed with PBS, incubated for 10 min with PBS/100 mM Tris and again washed with PBS before blocking for 1 h with 1% BSA in PBS. Cells were then incubated for 1 h with a 1:1000 dilution of the primary rabbit anti-VSG221 antibody in 1% BSA in PBS. After washing three times in PBS for 5 min each, cells were incubated for 1 h in the dark with a 1:500 dilution of the secondary goat anti-rabbit-Alexa 488 antibody in 1% BSA in PBS. Slides were again washed three times for 5 min in PBS and mounted using Vectashield with DAPI prior to imaging. Images were captured with an inverted fully automated DMI 6000B wide-field microscope (Leica Microsystems, Mannheim, Germany) equipped with a 63x glycerol objective (NA 1.3) (Leica Microsystems, Mannheim, Germany) and a CCD camera (PCO, Kelheim, Germany).

QUANTIFICATION AND STATISTICAL ANALYSIS

For the cell viability assay, the ratio of fluorescent, dead cells to non-fluorescent living cells was analyzed with a FACSCalibur Flow Cytometer (Becton Dickinson Bioscience, Franklin Lakes, USA). All experiments were performed in triplicate. FACS data for anti-His antibody, non-VSG2 coats, FITC labeled material and FAM-labeled material was analyzed in FlowJo (10.5.3) and statistical measurements were performed using Prism 8. To compare the negative controls (non-stained parasites and parasites only exposed to anti-His antibody) with stained samples a two tailed t test was used for statistical analysis. All p values can be found in Figure S2. Labeling was applied according to the PRISM definition of p value significance: $p \leq 0.05$ = *, $p \leq 0.01$ = **, $p \leq 0.001$ = ***, $p \leq 0.0001$ = ****.

For ensemble cell motility studies, trajectories were analyzed with the Imaris x64 software (Version 9.5.1, Oxford Instruments). For each condition and time point, track speed means and track displacement lengths were extracted from between 222 and 1410 individual trajectories acquired in two separate experiments. The distribution of individual data points for both sets of experiments is shown in Data S1. The median of the data together with the 25th and 75th percentile (bars) is presented in Figure 5B.

For FRAP experiments, the acquired data were analyzed according to Phair et al. and Hartel et al. (Phair et al., 2004, Hartel et al., 2015). In brief, at each time point the average fluorescence intensity of the bleached region of interest (ROI), the whole cell (I_{fg}) and the background (I_{bg}) were measured. A routine within the Offline Analysis Software (FEI Munich GmbH, Germany) used these data to perform a double normalization according to Phair with an exponential function then fitted to the normalized FRAP data. From this, both the half-recovery time of fluorescence (τ) and the ratio of mobile to immobile proteins (MF) were determined. The width of the bleached area ($2X$) was determined by analyzing the average distance between areas that were unaffected by bleaching. Once τ and X were known, the lateral diffusion coefficient D was calculated from $D = \frac{X^2}{4*\tau}$. In total 55 cells were analyzed for the untreated control cells and 48 cells for the $NB11_{VSG2}$ treated cells. Extracted diffusion coefficients and mobile fractions are presented in Figure 5E in form of a violin plot in order to show the distribution of the data. In addition the median over all values is shown together with the 25th and 75th percentile (bars). An unpaired, two-tailed Mann-Whitney test was used for statistical analysis using Prism (version 9.1.2). The determined p values are shown in Figure 5 with **** representing $p < 0.0001$.

Isothermal titration calorimetry

VSG and Nbs ($NB9_{VSG2}$, $NB11_{VSG2}$, $NB14_{VSG2}$ and $NB19_{VSG2}$) were dialyzed against PBS and PBS was also the buffer used for titration experiments. All experiments were performed with a MALVERN ITC machine (model: PEAQ-ITC cell) and data acquisition and integration were performed with the MicroCal PEAQ-ITC software. The cell concentration (VSG2) for all experiments was between

13-20 μM and the syringe (Nbs) concentration set to 120-240 μM. For NB9, NB11 and NB19 the cell temperature was set to 30°C, while $NB14_{VSG2}$ required a cell temperature of 20°C. Samples were centrifuged at 6000 x*g* for 7 min prior to measurement. All experiments were performed in triplicates. The weighted arithmetic mean of these data has been calculated to compare the samples.

Flow cytometry analysis of mutated NB11 incubated to the native VSG2 coat on *T. brucei*

$NB11_{VSG2}$ mutant (= $NB11_{mut}$, L100A/L101A/S103A) was added in 4-fold molar excess to 2×10^6 *Trypanosoma brucei brucei* cells in 200 μL cold HMI-9 medium and left at 4°C for 10 min with gentle shaking. The excess nanobodies were washed away with a cycle of resuspending in 2 mL cold HMI-9 medium followed by centrifuging at 6000 x*g* for 10 min. The washed pellets were resuspended in 200 μL cold HMI-9 medium and incubated with anti-His antibody (1:1000) in cold HMI-9 medium at 4°C for 10 min with gentle shaking. Samples were washed by a cycle of resuspending in 2 mL cold HMI-9 medium and centrifuging at 6000 x*g* for 10 min. Samples were resuspended in 200 μL HMI-9 medium for flow cytometry analysis (FACSCalibur, BD). Non-stained 2T1 cells and 2T1 cells only incubated with anti-His antibody were used as a control.